ACADEMIC YEAR 2013/2014

Corso di Laurea Magistrale in Ingegneria dell' Automazione

Scuola di Ingegneria Industriale e dell'Informazione

A comparative assessment of actuators for a novel track switch

Advisor:	Prof. Stefano BRUNI	(Politecnico di Milano)
Co-Advisor:	Dr. Roger DIXON	(Loughborough University)
Co-Advisor:	Dr. Nicholas WRIGHT, PhD	(Loughborough University)

Master of Science Thesis by

Andrea RONCHI (Matricola: 801247)

Contents

List of Figures

List of Tables

Abstract

Railway track switching provides the necessary flexibility to a rail network allowing the traffic to access many different routes. However, track switch introduces single points of failure and reduces the system capacity through rail vehicle control rules. Historically, minimal consideration is given to how the switch is designed. Switching practise, in fact, has evolved with safety as ultimate priority. Recently, however, capacity has become more critical. As the railway infrastructures are improved, over the years, traditional design of the track switches remains unchanged. The REPOINT research programme was started to investigate methods of increasing asset reliability for the track switching. In this context, a concept for a novel design has been developed, which allows multi-channel actuation by means of a novel actuation and locking mechanism.

The present work is focused on a comparative assessment of different actuator and drive assemblies for the REPOINT project. The target of the comparison is to identify and investigate a number of actuator and drive solutions and assess their impact on the performance of a REPOINT track switch. Three different actuators are analysed: an electro-mechanic BLDC actuator, an electro-hydraulic actuator and an electro-mechanic torque motor actuator. A model has been developed for each solution, by deriving it from a first physical analysis of its component parts. Then, a simple control design has been presented, showing later that they meet all the REPOINT performance requirements, as defined by previous research work performed by the group led by Dr. R. Dixon at the Loughborough University (UK). The final simulation results have been compared between the three actuators considering the most significant performances. For a more complete analysis these actuators are studied in three different scenarios, which would cover all the common situations of a railway network. Results show that each actuator and drive solution provides both advantages and disadvantages as for each particular performance taken into account.

Estratto

In genere gli scambi ferroviari forniscono la necessaria flessibilità ad una qualsiasi rete ferroviaria, permettendo al traffico di distribuirsi su più linee. Nonostante aumentino tale flessibilità, essi costituiscono, nello stesso tempo, un elemento critico di collasso della rete. A partire da questo, politiche di gestione del traffico limitano la capacità della rete, impedendo il transito dei veicoli ferroviari per intervalli di tempo consistenti. Storicamente, la tecnologia degli scambi si è sviluppata dando priorità alla maggior sicurezza, lasciando quasi invariati i meccanismi e i controlli dello scambio stesso, in quanto la capacità non era il fattore limitante nel progetto dello scambio. Ultimamente, però, il problema della capacità della rete ferroviaria è diventata più rilevante, rendendo, così, necessario uno studio più approfondito. Il progetto di ricerca REPOINT è stato concepito al fine di investigare sui metodi più opportuni per aumentare i parametri di affidabilità di uno scambio ferroviario. In questo contesto si inserisce il progetto di un scambio innovativo in via di costruzione. Questo nuovo dispositivo permette di avere migliori prestazioni attraverso un nuovo sistema di movimento e bloccaggio delle rotaie.

Il presente lavoro è costituito da un'analisi comparativa di diversi attuatori e trasmissioni, utilizzabili per il progetto REPOINT. L'obiettivo di questa analisi è quello di identificare e investigare diverse soluzioni, mostrando il loro contributo alle prestazioni dello scambio REPOINT. A questo scopo sono state analizzate tre diverse tipologie di attuatori: un attuatore elettro-meccanico con motore "BLDC", un attuatore elettro-idraulico, e un attuatore elettro-meccanico con motore "torque". All'inizio tutti gli attuatori sono stati ricondotti a modelli rappresentanti le caratteristiche fisiche dei propri componenti, senza entrare, però, in un'analisi approfondita di tutte le problematiche che questi dispositivi generano. Successivamente, lo stesso procedimento è stato seguito per la trasmissione meccanica di ciascuna soluzione. In seguito, un semplice schema di controllo è stato implementato per ciascun sistema, in modo da far rispettare tutti i vincoli ed i requisiti del programma REPOINT, i quali sono stati definiti in precedenti lavori da un gruppo di ricerca dell'Università di Loughborough (UK) guidato dal Dr. R. Dixon. I risultati finali delle simulazioni sono stati confrontati tra loro, tenendo conto degli elementi più significativi, quali velocità di attuazione, potenza elettrica richiesta e dimensione fisiche del sistema di attuazione. Per maggior completezza, le tre soluzioni

sono state studiate all'interno di tre scenari differenti. Questi tre scenari (stazione di London Waterloo, stazione di Derby e giunzione di Weaver) vogliono rappresentare una panoramica delle possibili e frequenti situazioni in cui gli scambi ferroviari giocano una funzione importante. Alla luce di questo studio, i risultati mostrano come ciascun attuatore, e relativa trasmissione, presentino vantaggi e svantaggi a seconda delle prestazioni prese in considerazione.

Chapter 1

Introduction

Over time, many parts of the rail facilities have been upgraded with new features, such as new rail cross sections, signalling methods, civil works and much more. Railway switches, conversely, has remained almost the same since the first railways were envisioned. In fact, only the switch actuation has changed, from mechanical rods and levers to more modern electrical or electro-hydraulic designs. So far, the basic mechanical design has remained unchanged, because the railway industry decided to give the ultimate priority to the safety problem, rather than to the railway network capacity. In recent times, however, capacity has become so important as to necessitate a detailed analysis. A representative case of this is the *HS2* (High-Speed 2) project [1], which is currently being developed in the United Kingdom. The purpose of this new rail link, indeed, is to create space on the overcrowded British network and let large numbers of people to move efficiently. In this innovative network metro-frequency services are proposed to run on 250 mph (400 km/h), crossing the boundaries of what current railway infrastructure is able to offer, in particular in terms of network capacity.[2]

The REPOINT research programme, performed by the *Control System Research Group* led by Dr. R. Dixon at the Loughborough University (UK), was started up, initially, in order to investigate methods of increasing asset reliability. Afterwards, a novel railway track switch was invented: this will, on the one hand, significantly increase capacity, and on the other hand, also provide advantages in terms of safety. A concept demonstrator is under construction, in order to provide preliminary, but significant results, which show the benefits of this novel design on the railway capacity.

In this context, the current work is a preliminary analysis of different actuation solutions, which may led to a well-performing railway switch. Three different actuators are taken into consideration, in order to provide a reasonable comparative assessment: an electro-mechanic actuator with BLDC motor, an electro-hydraulic actuator, an electro-mechanic actuator with a torque motor. At the same time, three real scenarios are

selected (London Waterloo Station, Derby Station, Weaver Junction), with the purpose to show the possible impact of each different solution on an existent segment of the network.

All the actuators and relative drive solutions are represented in simplified models, which describe the main physical behaviours of each device. In addition to this a control scheme is designed, with the aim of providing the desired movement to the switching rails. Proportional (P) and proportional-integrative (PI) are the control strategies adopted in this work. The whole amount of models and control designs are developed using MATLAB SIMULINK®.

Final simulation results reveal that each actuator offers advantages according to the considered scenario, but also presents several disadvantages. For this reason, it is not possible to identify a unique best solution. Thanks to these data, however, it is possible to show, for each situation, which actuator represents the best solution.

The present work is divided into seven chapters. After this introduction, in *Chapter 2*, the reader is introduced through a short description of the REPOINT research programme and a more detailed structure of the present work. Then, in *Chapter 3* all the models for each actuator and drive solution are presented. In all solutions there is a common mechanical part, which is discussed separately in *Chapter 4*. In *Chapter 5* the control designs used in the simulations are illustrated. From the work, several conclusions can be drawn and constitute the discussion of *Chapter 6*.

Chapter 2

The REPOINT Project

2.1 State of art

One of the most important parts of a rail network is the switch, also called turnout or point in the UK network. In fact, this particular system increases the flexibility of a rail network, letting the traffic access many different routes, typically from two to three. This mechanical installation is also important, because of its fragility. Switches represent a single point of failure and this also entails consistent constraints to the network capacity, due to the design of the turnouts and the control operation associated to it.

2.1.1 Traditional design

The general layout of a typical single turnout is composed of a *switch panel* and a *crossing panel* connected by a *closure panel*. The direction of the movement is changed in the switch panel part, which consists of two movable *switch rails*, *switching machines* and two *stock rails*. Stock rails are the non-moving parts of the point and they are placed on either side of the track. Two switch rails are able to move inside these fixed rails. These movable rails are specially shaped and machined to the *switch toe*, which is a sharp tip mounted at one end, and the *switch heel*, with the same rail cross-section as a stock rail, at the other end. These blades, also known as *switch tongues*, have the task of guiding the rail vehicle through the turnout and deciding if it will continue on its route or change it. The switch rails are moved by a switching machine, the actuator, and held in the correct position by two *stretcher bars*. The actuator is the device that controls this movement, and is generally located in the line-side, but in some cases it can be placed within the stock rails or among the switch rails.
A constant cross-section closure rails, called closure panel, is the part which links the switch panel to the crossing panel.
The last part of the point is the crossing panel, where the two tracks intersect at the same

level. The rails form a "V" shape at the *crossing nose* and with *wing rails*, also known as *wings*, at each side of the crossing nose, *check rails*, also called *guard rails*, and stock rails compose the crossing panel. The continuous rails are interrupted at the crossing point to allow, for a wheel flange, to pass the intersecting rails. In order to bridge this gap, wings rails are installed, guiding the wheels across the rail discontinuity. In the opposite side of the crossing nose, also called the *frog*, two check rails are placed on the tracks, preventing the opposite wheel flange from taking the wrong path at the crossing gap and from striking the crossing nose.
The actuator mechanism drives the moving bearers from the starting position to the final one. After this, a lock system is activated, which blocks the rails in the final position. Only when this movement is complete a signal is sent to the traffic control unit allowing trains to pass through the switch.

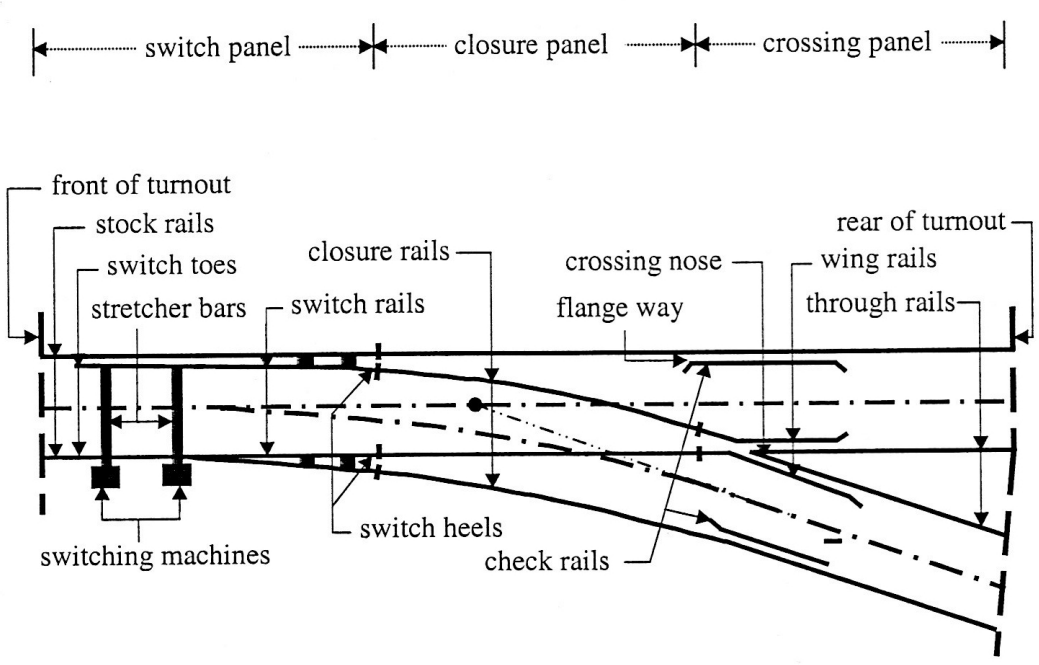

Figure 2.1: Typical *'traditional'* switch arrangement [3]

Figure 2.2: Typical example of a long turnout [4]

2.1.2 Railway capacity

Railway capacity is one of the most important characteristics of a railway network. Capacity represents the amount of rail traffic, which the network could support in a given time interval. It is a function of several components. One of these is the turnout by simply looking at the history of the railways infrastructures. Historically, the ultimate priority for a switching practise is devoted to safety, but over recent years, capacity has become more critical.[2] Thus, if previously switches had rarely been the limiting factor, recently they have become more important, demanding a more detailed analysis.
In the course of time, rail network is changed in many different part of its infrastructure, such as new cross-sections, signalling methods, civil works, etc. It is not possible to report the switches in this list. Indeed, over time, points have remained unchanged, since the first railways were conceived. In these years, only the switch actuation has changed by replacing the mechanical rods and levers with electrical or electro-hydraulic designs. Nevertheless, these innovations have not significantly contributed to an increment in the network capacity.
Furthermore, network capacity is decreased by a number of factors; one of the more important is the switch failure. In general, when a failure signal is detected, a control rule is activated, and, depending on different jurisdictions, can cause the entire closing of that particular junction or station. A turnout failure, in fact, could mean different problems, from the less dangerous, as not properly working sensors, to the more dangerous, as rails blocking in an intermediate position between the two routes. This last problem is the most dangerous one, because if a switch blocks in an intermediate position, or is not locked in a safe and final position, the risk of derailment increases exponentially. This is one of the reasons why the entire junction or station is closed by the authorised personnel.[5] This closure heavily decrease the capacity of the rail network, because all

the rail vehicles are forced to stop or change the route.
Over years, in order to prevent these failures, a few devices are adopted. In particular, the current trend in the rail industry is to increase the condition monitoring and condition based maintenance.[5] In this way it is possible to avoid most of the dangerous situations, which have the biggest impact on the network capacity. Although this is a good compromise, doing these inspections and maintenances requires an interruptions of the traffic, and so, again, a decrease in the capacity. The control inspections and maintenances can be brought back to two categories: regular and unplanned. The first one is a planned action and there is a current trend in rail industry, which aims to manage these types of operations during periods when less interferes with rail traffic. The unplanned, instead, are the worst, because they force the authorised personnel to immediately block the traffic in that junction or station, decreasing significantly the network capacity. Another trend to reduce failures, or decreasing their impact on the railway capacity, is utilising redundancy.[5] This solution is heavily utilised in other industries such as aeronautic or aerospace, where safety-critical systems are present. This trend is, however, not particularly developed yet, even if, in principle, it may increase the railway capacity considerably.

2.2 REPOINT tasks and requirements

The REPOINT research programme was started to investigate how to increase the railway capacity and how to improve network delay performance through the application of technologies in common to other industries. With this purpose a novel design of a railway track switch is being designed.
The idea is to build a system constituted by three parts, as shown in Figure 2.3.

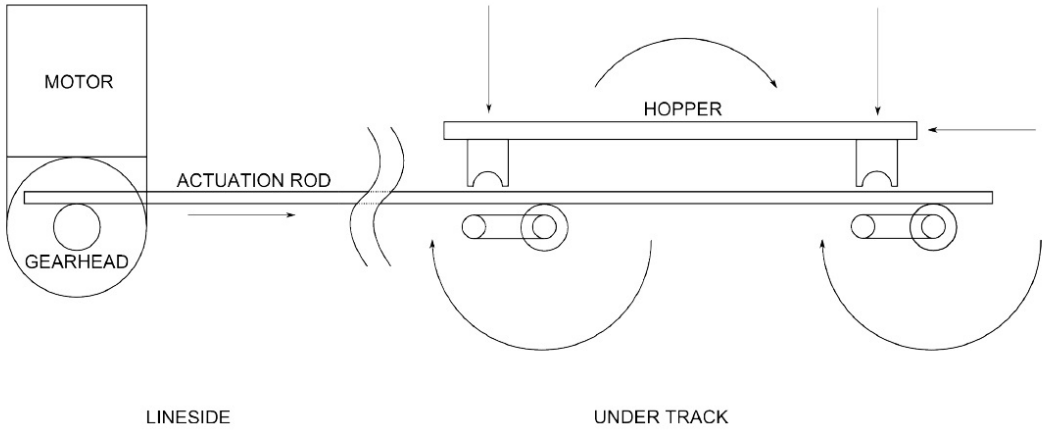

Figure 2.3: Mechanical arrangement of the actuation mechanism within a single actuator-bearer [6]

The first part is a cams and *hopper* assembly, where the blades are fixed and moved. Then, a mechanical linkage connects the cams to the actuator.
The laboratory demonstrator, which is being built for this project, is shown in Figure 2.4.

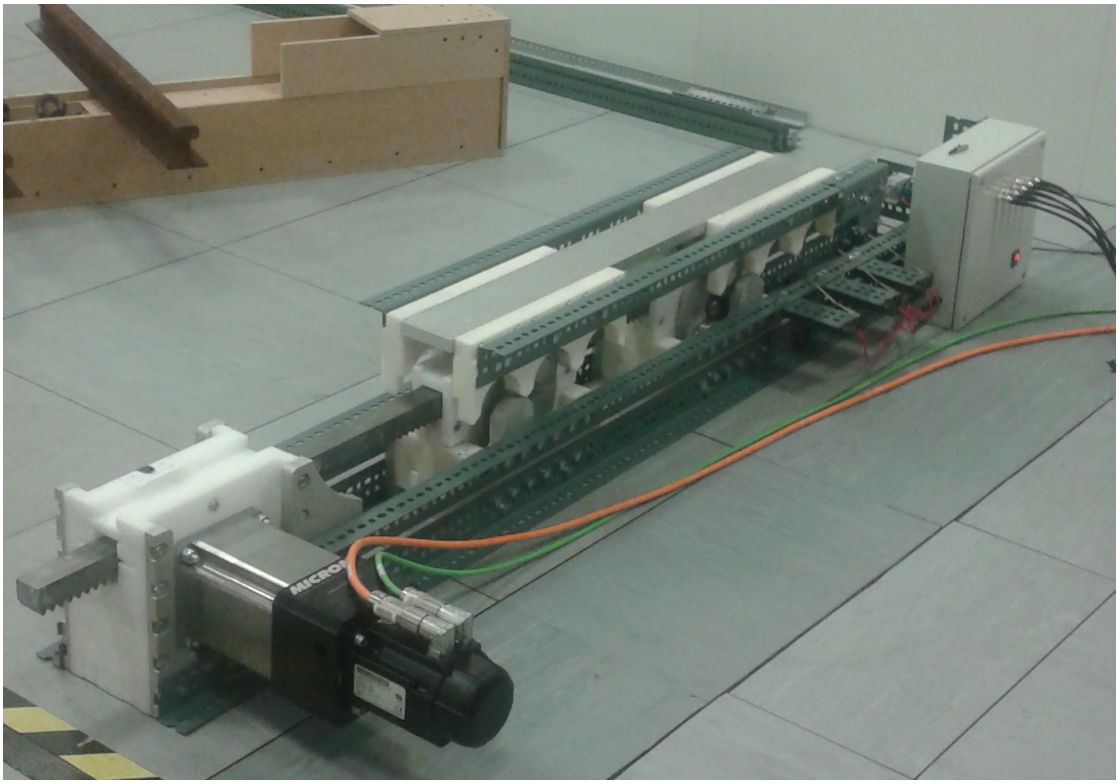

Figure 2.4: REPOINT laboratory demonstrator, illustration courtesy Loughborough University

As one can see in Figure 2.4 the hopper is moved through four cams mounted under it. The cams are driven by a common rack and pinion system. Each cam is provided with a protrusion upon its end, which features with its specific pinion. The cams are placed below the hopper. An electric motor drives the rack through a gearbox and a spur gear, providing the forward or the backward motion. In this demo, the switch rails are not considered. A system of sensors are placed in the final part of the turnout controlling the rack position.
The final installation will present the switch rails directly mounted on the top surface of the hopper, perpendicular to the motion direction of the rack. A cut-out on the underside of the hopper engaging with a stationary protrusion mounted to the base of the actuator-bearer housing provides the locking in either position. Therefore, the movement between two positions is done by firstly lifting out the rails of their locking *'groove'*, and then by being dropped in the final position through a semi-circular path. In this way the track is accurately aligned in each position.
However, considering the high torque this actuator has to provide to move these switch rails (in the order of thousand newton-meter), a redundant system is preferable. For this reason, two or three of these actuator bearers are thought to be present on a single REPOINT switch. In this way, the whole safety of the entire switch is increased, and, at the same time, the torque which has to be provided by each system is lower.
This novel switch is designed reaching some different targets on the mechanical, electrical, diagnostic and fault detection performances and requirements.

2.2.1 Mechanical performance considerations

From a mechanical point of view there are a few considerations that have to be done. Firstly, this system should be suitable to being used in a programme called *'Modular S&C'* [6]. Among the targets of this programme there is one, which is to reduce the installation time of switches to a single evening possession by pre-assembling the track components of the switch nearby and by installing them using specially designed tilting wagons. This is desirable, because initial placement and end-of-life replacement require an entire blockage of the line for many hours [5]. The new point, discussed in this work, suits the fitment times achieved by this method. In fact, all components are mounted inside the switch rails, allowing the turnout to potentially be delivered and then *plugged and played* directly in the desired place.
The modular mechanical arrangement and parallel functional channels enables, also, to decrease the necessity and the rapidity of planned maintenance.
Furthermore, turnouts need to be protected from operating environment. In fact, turnouts are subject to high temperatures, which can reach upwards $70°C$ in summer, to flood, or to freeze in winter. On the rails there could be also numerous sources of contaminants,

like abrasive coal dust falling from wagons, fuel oil and ballast fragments. REPOINT switches have the peculiarity of not to have flange gap to grow or shrink, comparing to traditional points and for this reason are less affected by this problem.
Lastly, a fundamental mechanical requirement is about safety. In this way a REPOINT switch increase significantly this performance. In fact, compared to traditional turnouts, where with a sufficiently strong lateral force, in the order of several tonnes, the lock could be broken, or where stretcher bars are still present with their failure danger, this novel turnout offers an important improvement. Indeed, no more stretcher bars are present, and all locking is dependent upon the rails being forced into their locking groove. In this way, the forces to break these locking have to be in the order of several tonnes, which are hard to achieve in the vertical plane. In fact, the load from a wheel set is almost exclusively in the opposite direction, downwards.

2.2.2 Electrical and control performance requirements

Concerning the electrical and control requirements there are few aspects, which are improved by this novel switch. Other constraints, instead, are given for a robust control design. The first aspect is the electrical interface, which is compatible with the pre-existing signalling infrastructure. The second one is the actuation time. The maximum operation time allowed for a railway point in the UK is around eight seconds; the REPOINT project tries to complete this movement in around two seconds, with respect to traditional switches, where the movement is completed in a range between two and four seconds. This improvement could increase the railway capacity. Another aspect is the robustness and the fault tolerance. In the operation of a traditional turnout there are several degrees of variability, as parameter drift, non-linearities, manufacturing differences, variable environmental conditions, and other factors. At a design stage these disturbances or uncertainty had to be taken into account. For a classical frequency domain control design, at least a 60°phase margin in the system's closed loop response and a 6 dB gain margin is required [7].
It is also important to maximise the operational lifespan by controlling different variables such as thermal and torque load on each bearer. Traditional switch, generally, uses single phase DC brush motors, on the contrary the REPOINT switch chooses an electronically commutated DC brushless motor (BLDC). This choice eliminates the presence of brushes, which requires more maintenance and, furthermore, they are not easy to replace. Moreover, an efficient motor commutation and effective motor current control should be designed in order to minimise the impact of this new turnout on the network infrastructure. The last aspect concerns a simplified design of the control part of the switch in order to minimise the danger of error, avoiding difficult procedures to set up and control the switch.

2.2.3 Diagnostics and fault detection

When a system or a plant is set up a tool, which recognises abnormal behaviour in the process, is needed. This tool is a condition monitoring scheme, also known as Fault Diagnosis and Isolation (FDI) [6]. In literature, many papers have been written reviewing the most common FDI techniques [6]. One of these techniques is particularly suitable for the REPOINT project, and is a quantitative model based on condition monitoring. When detailed design information is available, as in this project, this class of technique could be used successfully. From those reviews, one may see that, when the dynamics of a plant can be mathematically described, this condition monitoring scheme can provide an accurate and timely diagnostic information.
Concerning fault detection, a FMECA (Failure Mode Effects and Criticality Analysis) procedure is adopted using a particular scale of failures (Catastrophic, Critical, Major, Minor). FMECA is a systematic analysis technique of a system for failure analysis [6].

2.3 Actuators comparison

The last steps of the REPOINT project consists to build a laboratory demonstrator to validate the previous studies and prove the increase of the railway capacity. As explained before, this novel switch is composed of three mechanical subsystems, a cams and hopper assembly, a mechanical linkage and an actuator. The actuator chosen for this demonstration is a BLDC motor, as explained before, because of its similarity with the traditional ones, which are more consolidated than other devices (e.g., electro-hydraulic actuators). Nevertheless, considering the fact that is a novel design, having a comparative assessment of the actuators is desirable. It is possible to have some improvements choosing a different actuator. For instance, it is possible that, with different scenarios, other types of actuators offer better performances.
In this work a comparison between three different types of actuators is made. From the entire overview of all the possible actuators, only three are considered here:

- BLDC motor
- Electro-hydraulic actuator
- Torque motor

The comparison does not aim at definitely answering to the problem of the choice of the actuator. Conversely, it wants to show different solutions. For this reason, all the selected actuators and controls allow to give a qualitative overview of different way to drive this novel switch. Hence, these devices and their controls are not studied in detail, because the target of this work is to provide a comparative assessment of the actuators.

Moreover, the laboratory demonstrator actuator had already been chosen, as explained before. Providing performances data from different actuators will give a more complete idea of the real impact of this novel design on the railway network.
In order to provide these data, a few elements, on which it is possible to do a comparison, have to be decided:

- Velocity of response
- Electric power demand
- Physical dimensions

These are the factors that mostly affects the actuators performances. Of course, the velocity is important, since it is one of the factors that influences the railway capacity. The electric power demand is a notable parameter that becomes important when more switches are placed in a junction or in a station. The last element is fundamental to understand how much space has to be allocated to the switch, and is obviously related to the particular scenario.
Other aspects of the switch that were discussed in the previous sections do not significantly change among the different actuators or require a more deep analysis. For instance, the safety of a REPOINT switch, which is the greatest improvement of this novel switch, is not considerably dependent on the type of actuator. This means that changing the actuation system will not influence this fundamental improvement. In fact, the cams and hopper assembly is the most important responsible for the whole system safety and it remains the same among the considered actuators. Concerning the fault detection and also all the other aspects, a more accurate and focus inspection is needed. These elements are not taken into account in this work, also because are less important than the considered ones.

2.3.1 Structure of the work

Data are obtained by a simulation of the behaviour of the three different actuators. Each actuator is described by some simple and general equations representing the physical behaviour of these devices. These equations are implemented in a model using MATLAB SIMULINK®. After this, a model for the mechanical linkage for each actuator design is built, starting, one more time, from the physical characteristics of the components, and directly connecting them with the previously described model. Mechanical linkages present a common component, the rack, but differ from each other in the way this actuation rod is moved. At the end, a model for the cams, hopper and a single switch rail is made. This particular model is the same in each actuator design, and for this reason it will be treated in a separate chapter. This model consists of the cams, which are spun

by the linear movement of the rack through the pinions, as explained before. This model will receive the cam pinion torque as input from the mechanical linkage of each actuator. The general scheme is depicted in Figure 2.5.

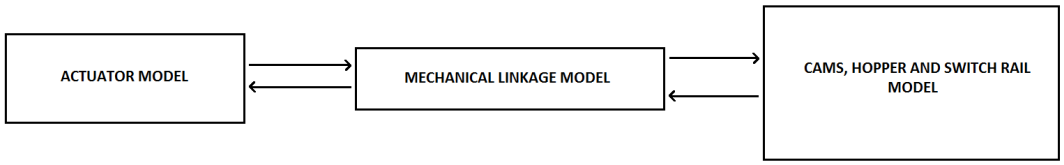

Figure 2.5: General scheme of REPOINT switch analysed in this work

After this modelling part, a simple control design is performed, as explained in the previous sections: firstly considering the particular requirements and design constraints of each actuator, then making some other considerations.
Finally, after all the needed simulations have been run, and all the data collected, these are used for the comparison of the final results.

Chapter 3

Actuator Models

In this chapter all the actuator models and the related mechanical linkage models are being presented. The aim is to provide an easily description of the physical behaviour of the device and of the mechanical transmission for each actuator system. The mechanical linkage is what transfers the movement, provided by the actuator, to the cams and hopper assembly (i.e., rack and pinion), which is the common part of the REPOINT switch among the solutions, as explained before. For this reason, it is treated separately in Chapter 4.
All the actuation systems are driven by the voltage applied to the correspondent electric motor as an input, and provide a cam pinion torque to the cams and hopper assembly as an output.
Before starting the description, a general consideration is made. All the friction coefficients for the mechanical parts are neglected: these parameters need to be physically measured or estimated from the real plant. Considering the schedule of the project, this part has not been completed yet.

3.1 Electro-mechanical actuator

The first family of actuators being analysed is the electro-mechanical actuator family. Electro-mechanical Actuators (EA) are the most common actuators in railways switches. This is for their reliability and their easy implementation. EA are normally composed of an electric motor and a variety of mechanical components.
The EA structure chosen in this work consists of a brushless DC motor linked to a gearhead. This gearhead is a high precision planetary gearbox, which allows to transfer the desired torque to the remaining part of the system.
The structure is depicted in Figure 3.1.

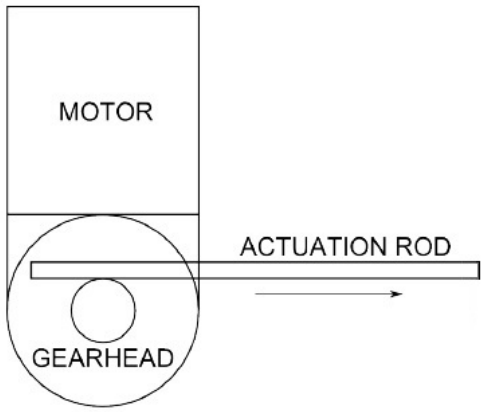

Figure 3.1: Scheme of the proposed electro-mechanical actuator

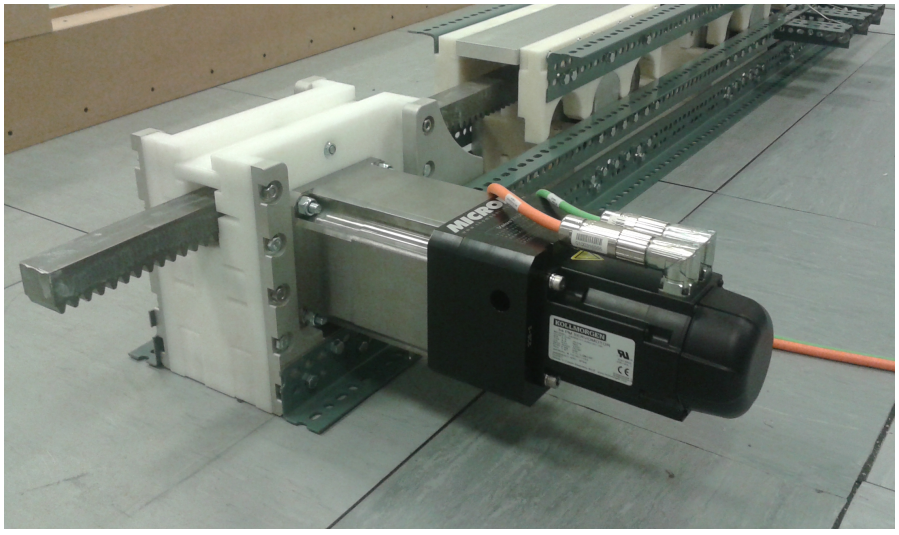

Figure 3.2: Proposed REPOINT electro-mechanical actuator, illustration courtesy Loughborough University

A top level scheme of the actuator model was made via MATLAB SIMULINK®and is shown in Figure 3.3.

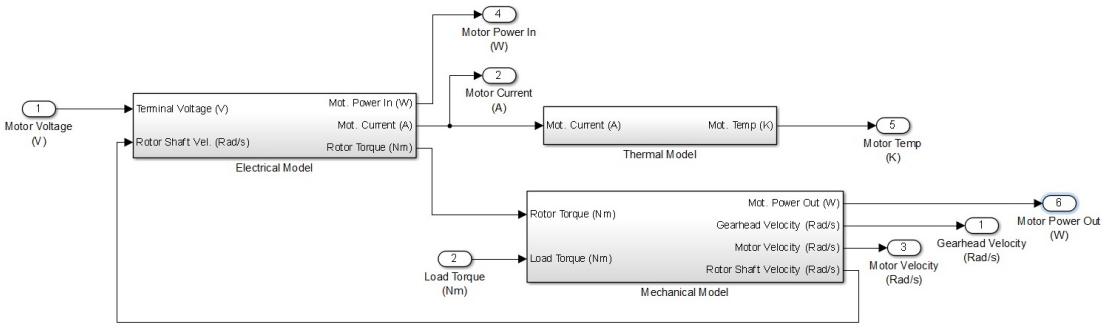

Figure 3.3: EA — Motor and gearhead model scheme — Top level

There are two inputs[1], which are the motor voltage (V) and a load torque (N·m); and six outputs, which are gearhead velocity (rad/s), motor current (A), motor velocity (rad/s), motor power input and output (W), and motor temperature (K).

3.1.1 Model

Electric motor

The electric motor is the most important part of this actuator. It provides the torque, moving the rail pair. In particular, a brushless DC motor, also called BLDC motor, is a synchronous electric motor, which spins the rotor by applying a three phase voltage supply to the stator. This movement is achieved by giving an electronic commutation provided by motor drive. This commutation is the cause of an undesired occurrence, known as torque ripple. In many cases this effect is significant, but concerning the purpose of a REPOINT rail switch, it is reasonable to neglect it. For this reason, it is not taken into account in this model.

Behaviours of a typical BLDC are described by these simple equations:

$$V = R_a \cdot I + L_a \cdot \frac{dI}{dt} + E \tag{3.1}$$

$$E = k_e \cdot \Omega_m \tag{3.2}$$

where V is the armature motor voltage, R_a is the armature resistance, I is the armature current, L_a is the armature inductance, E is the back emf, k_e is the back emf constant, Ω_m is the angular position of the rotor.
Concerning the motor torque, the relationship between current and torque is:

$$T_m = k_t \cdot I \tag{3.3}$$

[1]Hereinafter, any unit of measurement appearing in brackets will specify the dimensions of the physical quantity preceding it.

where T_m is the motor torque, k_t is the motor torque constant and I is the armature current again.

The electrical part of the motor is presented in Figure 3.4, where the inputs are the motor voltage (V) and the rotor shaft velocity (rad/s), and the outputs are the motor power input (W), the motor current (A) and the rotor torque (N·m).

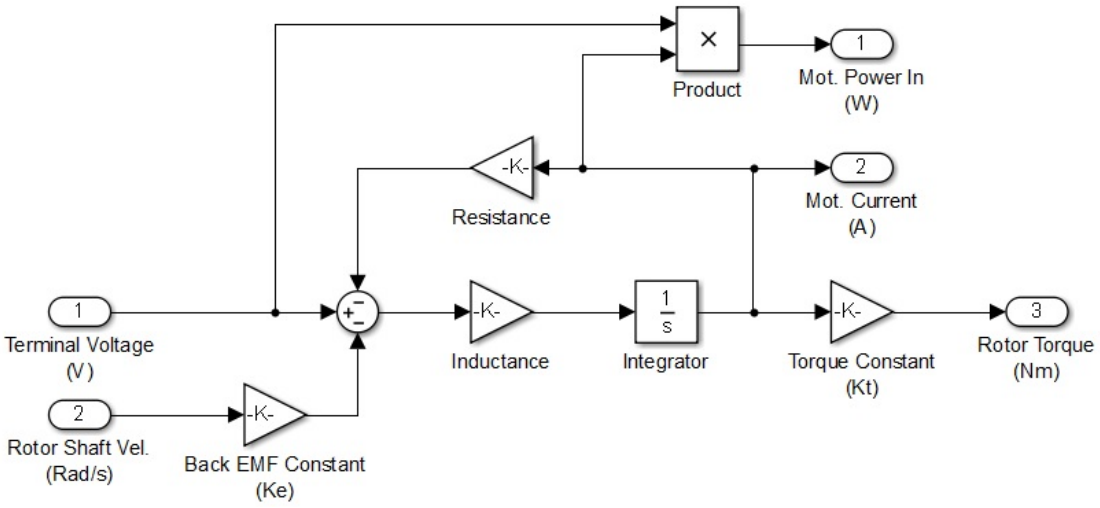

Figure 3.4: EA — Motor and gearhead model scheme — Electrical motor

The mechanical model of this actuator is obtained by solving a simple torque balance, and it can be seen in Figure 3.5, where the rotor torque (N·m) comes from the electrical model of the motor, and the load torque (N·m), which comes from the mechanical linkage, to be discussed later (gearhead torque output of the mechanical linkage model). The motor power output (W) and the velocity (rad/s) gearhead, rotor shaft and motor are the model outputs.
By performing a simple torque balance it is possible to describe the mechanical output.

$$T_m - T_g = J_m \frac{d^2\theta}{dt^2} + D_m \frac{d\theta}{dt} \tag{3.4}$$

where T_g is the gearhead torque and D_m is the motor friction constant.

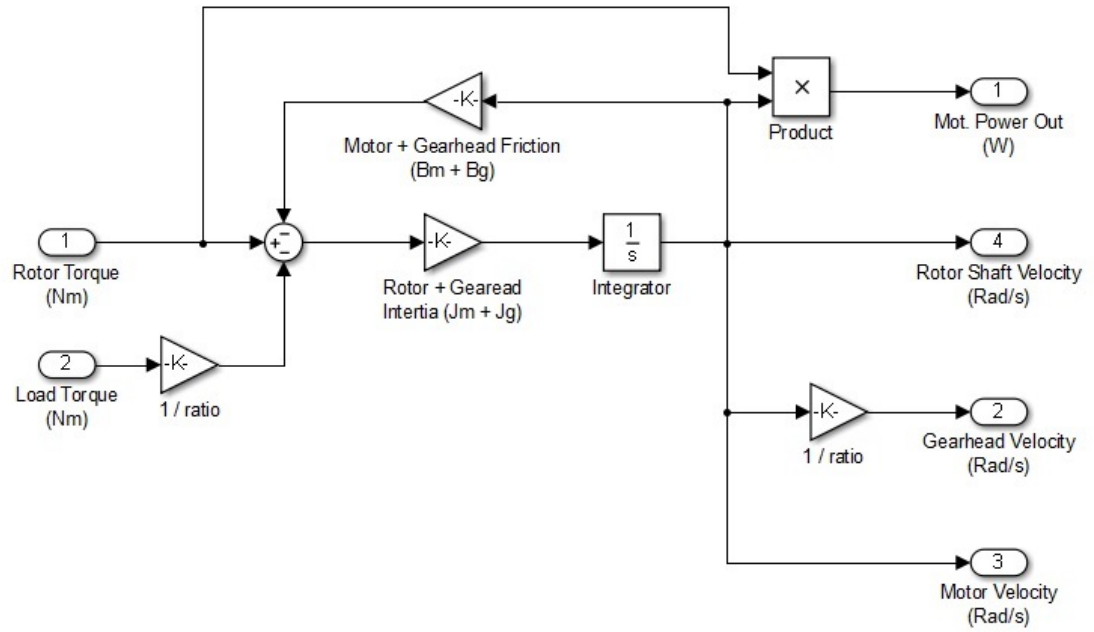

Figure 3.5: EA — Motor and gearhead model scheme — Mechanical model

Finally, a consideration about thermal behaviour of a BLDC follows.
The relationship, which describes the motor temperature (τ_m), is:

$$\frac{\tau_m}{dt} = \frac{I_a^2 R_a - K_h \tau_m}{C_m} \tag{3.5}$$

where K_h is the motor head dissipation constant and C_m is the heat capacity of the motor.
The thermal model is represented in Figure 3.6, where the motor current (A) comes from the electrical model of the BLDC and the motor temperature comes out from the top level model.

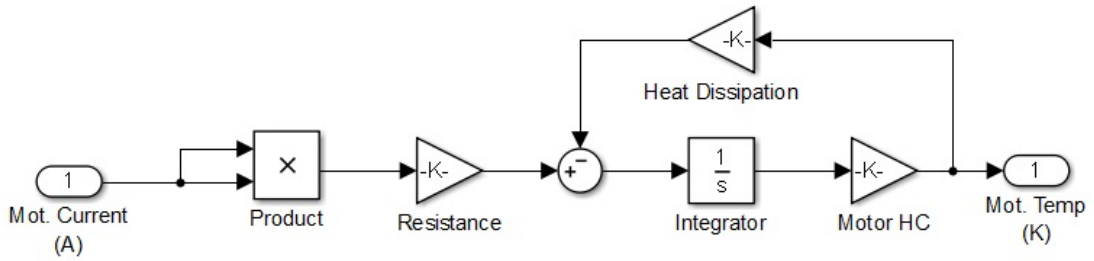

Figure 3.6: EA — Motor and gearhead model scheme — Thermal model

3.1.2 Parameters

The components and the parameters used to build the actuator model are listed in the following tables. Most of the values are taken from manufacturers' datasheets. The other remaining parameters are estimated basing on data from components of similar performance.
These values are marked with an asterisk.

Type	**Manufacturer**	**Part No.**
Brushless DC Servo Motor	Kollmorgen	AKM44H
Planetary Gearhead	Kollmorgen	VT014-070

Table 3.1: EA — Motor and gearhead component list [8][9]

Parameter	**Symbol**	**Magnitude**	**Units**
Motor armature inductance	L_a	9.1	mH
Motor armature resistance	R_a	2.23	Ω
Motor back EMF constant	K_e	68	V/k_{rpm}
Motor torque constant	K_t	1.06	Nm/A
Motor viscous damping	B_m	0.021	Nm/k_{rpm}
Motor inertia	J_m	2.7	Kg cm^2
Motor heat dissipation factor	K_h	0.7	W/K
Motor heat capacity*	C_m	0.000576	K/J
Gearhead viscous damping*	B_g	0.01	Nm/k_{rpm}
Gearhead inertia	J_g	2.85	$Kgcm^2$
Gearhead reduction ratio	n	70	Unitless

Table 3.2: EA — Motor and gearhead parameters [8][9][10]

Motor and gearbox were selected for the lab demonstrator. For this reason they were chosen in order to satisfy the task in a plentiful way.
Concerning the physical dimensions, this actuator is able to occupy a small area. This, due to the way these components are made. In fact, the gearhead sits flush with the end of the motor.
In Table 3.3 all the geometric dimensions are reported.

Parameter	**length x width x height**	**Units**
DC Motor	146 x 130 x 147	mm
Gearbox	262 x 141 x 147	mm
Total dimensions	408 x 141 x 147	mm

Table 3.3: EA — Motor and gearhead dimensions [8][9]

3.2 EA mechanical linkage

An easy way to connect the BLDC to the cams is to consider a rack and pinions assembly. In order to transfer the torque provided by the motor to the rack and pinion assembly, a mechanical linkage is needed. A possibility consists of using a gearbox, which allows the physical linkage. At the other side of the rack, other pinions screwed directly on the cams transfer the movement of the motor to the cams and the hopper.
This particular solution is built in the laboratory demonstrator and is shown in Figure 3.7.

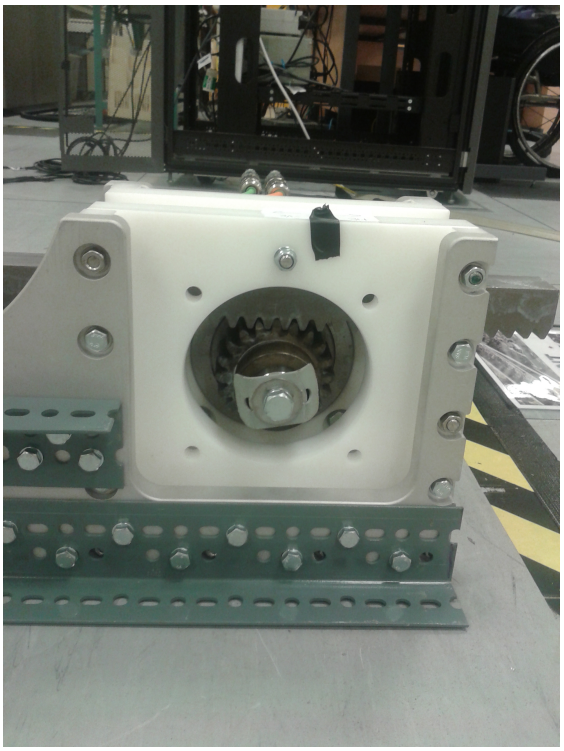

Figure 3.7: Laboratory demonstrator mechanical linkage (Spur gear and rack), illustration courtesy Loughborough University

3.2.1 Model

Gearhead description

The BLDC motor is connected to the gearbox by a short shaft. The output shaft torque is described by:

$$T_s = (\omega_m - \omega_{gi})\, c_s + \int (\omega_m - \omega_g)\, k_s \tag{3.6}$$

where T_s is the shaft output torque, ω_{gi} is the gearhead input speed, c_s is the shaft damping constant, and k_s is the shaft stiffness.

The output gearhead velocity can be found by making a torque balance.

$$T_s - \frac{T_{ma}}{n} = J_g \frac{d\omega_{gi}}{dt} + n\omega_{go} B_g \tag{3.7}$$

with

$$\omega_{go} = \frac{\omega_{gi}}{n} \tag{3.8}$$

where T_{ma} is the mechanical assembly load torque, ω_{go} is the gearhead output speed, n is the gearing ratio, and B_g is the gear damping constant.
The angle θ_{go} of the gearhead output, can be obtained by integrating ω_{go}. Another important behaviour of the gearbox is the gearhead temperature. It can be found by solving:

$$\frac{d\tau_g}{dt} = \frac{T_s\omega_{gi} - T_{ma} - K_g\tau_g}{C_g} \tag{3.9}$$

where τ_g is the gearhead temperature, K_g is the gearhead heat dissipation factor, and C_g is the heat capacity of the gearhead.

Lumped Parameter Description

By looking at the real plant a consideration can be made. The shaft taken into account is short and, even if it twists, it doesn't reach great degree. Indeed, the gearhead matches properly with the shaft. Therefore, it is possible to neglect it in the simulation model. A simple way to do this, is to define lumped parameters of motor and gearhead.
The previous torque balance can be rewritten, by lumping all the frictions and inertias parameters in this way:

$$T_m - \frac{T_{ma}}{n} = (J_m + J_g)\frac{d^2\theta}{dt^2} + (B_m + B_g)\frac{d\theta}{dt} \tag{3.10}$$

The drawback of this approach is that is one cannot solve the gearhead temperature equation. However, by considering the whole system it can be noticed that the thermal performance of the motor is more relevant than the gearhead one, in particular concerning design and control of the plant.

Rack and pinion Model

The rack and pinion model is the mechanical system chosen to connect the cams to the motor. The equation of motion, which represents this structure, is a discontinuous

function. This due to the backlash effect.

$$f(x) = \begin{cases} 0 & \text{for } \theta_g < \theta_m \\ \dfrac{T_{gp}}{R_g} - \dfrac{T_h}{R_h} = M_{ma}\dfrac{d^2x}{dt^2} + B_{ma}\dfrac{dx}{dt} & \text{for } \theta_g \geq \theta_m \end{cases} \tag{3.11}$$

where x is the displacement of the rack, R_g and R_h are the gearhead and cams pinion radius, T_{gp} is the gearhead torque, T_h is the torque from the cam pinion, B_{ma} is the rack assembly friction coefficient, M_{ma} is the mass of the rack assembly, θ_g is the angular position of the gearhead, and θ_m is the angle at which the pinion engages with the rack. The backlash effect may be reasonably neglected, because the materials of the components are less affected by that problem. In this way, for the final model, only the second equation of System 3.11 is considered.

The torque exerted by both the gearhead and cam pinions is a function of their torsional stiffness:

$$T_{gp} = k_g \left(\frac{x}{R_{gp}} - \theta_{go} \right) \tag{3.12}$$

where θ_{go} is the angle of the gearhead, calculated before, and k_g is the gearhead torsional stiffness.

In the same way, the cam pinion torque may be represented.

$$T_h = k_c \left(\frac{x}{R_h} - \theta_c \right) \tag{3.13}$$

where θ_c is the angle of the cam pinion and k_c is the cam pinion torsional stiffness.

The treated linkage is shown in Figure 3.8, where the gearhead velocity (rad/s) coming from the actuator model and the cam velocity (rad/s) coming from the cams and hopper model, which will be discussed in Chapter 4. Gearhead torque (N·m), rack position (m) and cam pinion torque (N·m) are the outputs of this linkage model.

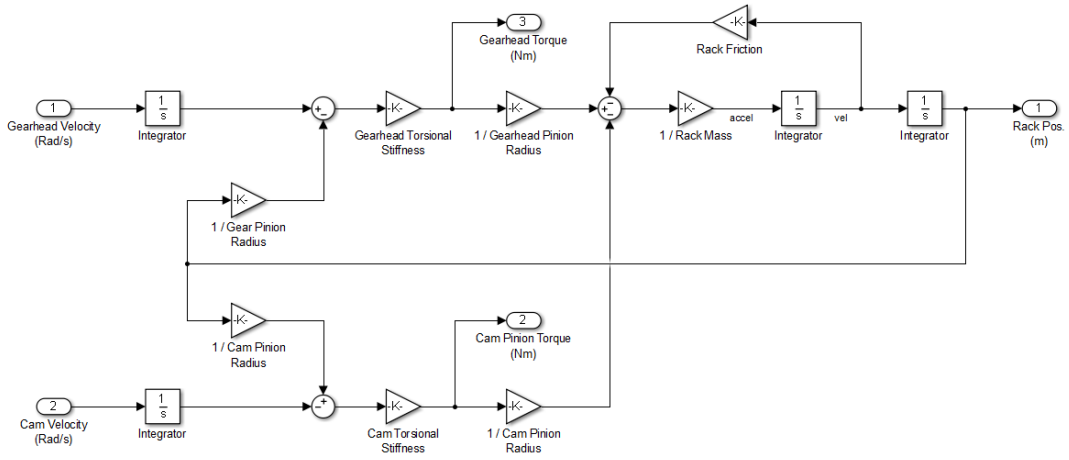

Figure 3.8: EA — Rack and pinion model scheme

3.2.2 Parameters

As in the previous section, all the parameters of this mechanical linkage are taken from manufacturers' datasheets. If some of them are not available, an estimation is made according to the performances of similar components. The estimates are marked with an asterisk.

Type	**Manufacturer**	**Part No.**
Steel Pinion Gear and Shaft	HPC Gears	ST4-15
Steel Spur Rack	HPC Gears	CR4
Heavy Duty Steel Spur Gear	HPC Gears	YG4-20

Table 3.4: EA — Rack and pinion components list [11][12][13][10]

Parameters	**Symbol**	**Magnitude**	**Units**
Rack mass	M_{ma}	14.3	Kg
Rack friction coefficient*	B_{ma}	0	N/ms^{-1}
Gearhead pinion radius	R_g	0.04	m
Hopper pinion radius	R_h	0.03	m
Gearhead backlash	θ_m	5	Arc-min
Gearhead torsional stiffness	k_g	44.1	Nm/Arc-min
Hopper torsional stiffness*	k_c	40	Nm/Arc-min

Table 3.5: EA — Rack and pinion parameters [11][12][13][10]

3.3 Electro-hydraulic Actuator

The second type of actuators discussed in this work is the electro-hydraulic actuator. Electro-hydraulic Actuators (EHA) are characterized by their ability to impart large forces at high speeds and are used in many industrial motion systems. EHA are devices composed of three elements: motor, servo-valve and cylinder.

A typical EHA structure is made of an electric torque motor acting on a flapper assembly of a flow control servo-valve as shown in Figure 3.9. This movement causes the opening or the closing of the valve and allows the fluid to flow to and from the actuator. The fluid flows into a cylinder changing the chamber pressure. This variation in the pressure pushes the piston, which is directly attached to the rack. This movement makes the cams rotating.

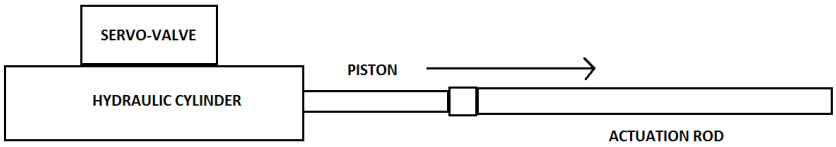

Figure 3.9: Proposed scheme of the electro-hydraulic actuator

Figure 3.10 represents a top level scheme of the actuator model built with MATLAB SIMULINK®.

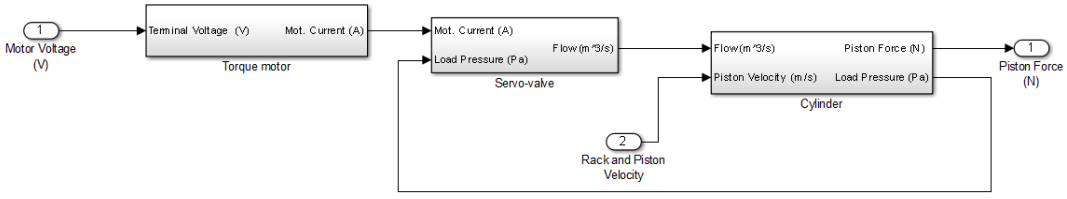

Figure 3.10: EHA — Servo-valve and cylinder model scheme — Top level

In this figure the inputs can be recognised , the motor voltage (V) and the rack (or piston) velocity (m/s), and the output, which is the piston force (N).

3.3.1 Model

Electric Motor

EHA are generally driven by torque motors. Torque motors are a high-torque DC motor with permanent magnet stators. The voltage applied to the excitation circuit induces an armature current, according to the common electro-magnetic laws. The mechanical torque is only a function of armature current. The torque has the aim to spin the flapper assembly of the valve. This is the way in which the flow rate of the valve can be changed, because the rotation of the flapper assembly causes a movement of the valve spool, which modifies the opening or the closing of the nozzles.
A typical servo-valve scheme is shown in Figure 3.11.

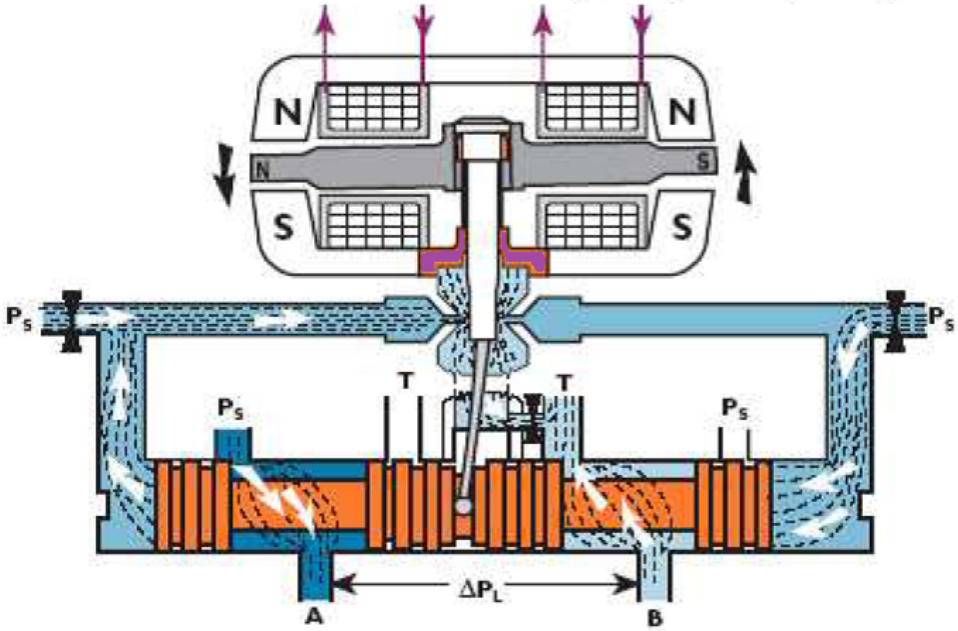

Figure 3.11: Typical servo-valve scheme [14]

The equations, which represent the features of this motor are the following:

$$V = R_a \cdot I + L_a \cdot \frac{dI}{dt} \tag{3.14}$$

$$T = k_t \cdot I \tag{3.15}$$

where V is the armature motor voltage, R_a is the armature resistance, I is the armature current, L_a is the armature inductance, Ω_m is the angular position of the rotor, T is motor torque and k_t is the motor torque constant.

The back emf is not taken into account here, because the motor considered in this

application is a little torque motor, thus its value is negligible compared to the other terms of Equation 3.14. For simplicity, the electrical characteristic may be modelled as a common L-R circuit. The transfer function between voltage applied and motor current is:

$$V = \frac{I}{L_a \cdot s + R_a} \tag{3.16}$$

This result is implemented in the model as shown in Figure 3.12, where the motor voltage (V) is the only input and the motor current (A) is the output.

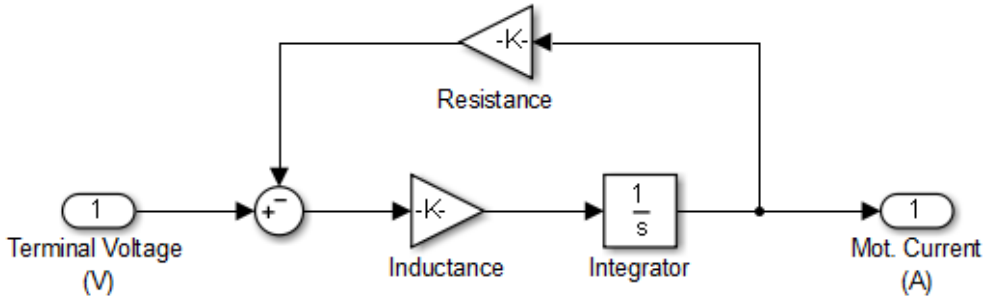

Figure 3.12: EHA — Servo-valve and cylinder model scheme — Torque motor

Servo-valve description

A flow control servo-valve is composed of several components as nozzle, orifice, spool, the latter made of lands (orange part in Figure 3.11, also called spool rod) and groves (the remaining parts of the spool), and many others. The typical behaviour of these devices is complex, due to some non-linearities. Fortunately, manufacturers tune all the parameters in order to guarantee a specific range of flow. In this way it is possible to represent the behaviour of this device considering only some simplified formulas [15].

The flow equation of the valve can be written as

$$Q = Ubc_d\sqrt{\frac{P_s - Psgn(U)}{\rho}} \tag{3.17}$$

where Q is the flow rate of the valve for steady-state operation, U is the input displacement applied to the spool rod using a torque motor considering also the valve lands are in the neutral (central) position $U = 0$, b is the land width, c_d is the discharge coefficient at each port, ρ is the density of the hydraulic fluid and P_s is the supply pressure of the hydraulic fluid.

P is the pressure difference supplied to the hydraulic actuator and, is also the pressure

provided by the load, and is denoted by:

$$P = P_2 - P_1 \tag{3.18}$$

where P_1 and P_2 are the pressures of the two chambers of the valve. In order to consider every direction of the flow a function sign may be considered.

Starting from this equation, a non-dimensional formula can be written.

$$\frac{Q}{Q_{max}} = \frac{U}{U_{max}} \sqrt{\frac{1 - P \operatorname{sgn}\left(\frac{U}{U_{max}}\right)}{P_s}} \tag{3.19}$$

where Q_{max} is the no-load flow rate of the valve, U_{max} is the maximum signal input.
It is common use, in servo-valve datasheets, to specify the no-load flow as rated flow. In a first analysis, leakage effect can be neglected. In fact, typical leakage flow profile presents an initial peak, when there is the commutation, and then it stabilises on a constant value, which is not relevant. The leakage effects may be considered only when the dynamics of the servo-valve is important considering the whole dynamic response of the system, but this is not case [16]. Another assumption made is about the system pressure supply, which is considered able to provide a constant pressure without any losses. Lastly, the input displacement U is considered proportional to the motor current, so that the flow rate of the servo-valve can be written in this way:

$$Q = Q_{nl} \cdot \frac{i}{i_r} \sqrt{1 - \frac{P}{P_s} \operatorname{sgn}\left(\frac{i}{i_r}\right)} \tag{3.20}$$

The choice of the proper servo-valve is made by looking principally to the performance of the system. In particular, according to what is said in the previous chapters, the servo-valve may provide the flow, which will be able to move the hopper in a certain range of time. This range is decided to be around two seconds, which guarantees a significant increase of the performances of the switch itself.
The scheme of the servo-valve model is shown in Figure 3.13, using the motor current (A), coming from the torque motor model, and the load pressure (Pa), coming from the cylinder model, as inputs and the only valve-flow (m^3/s) as output.

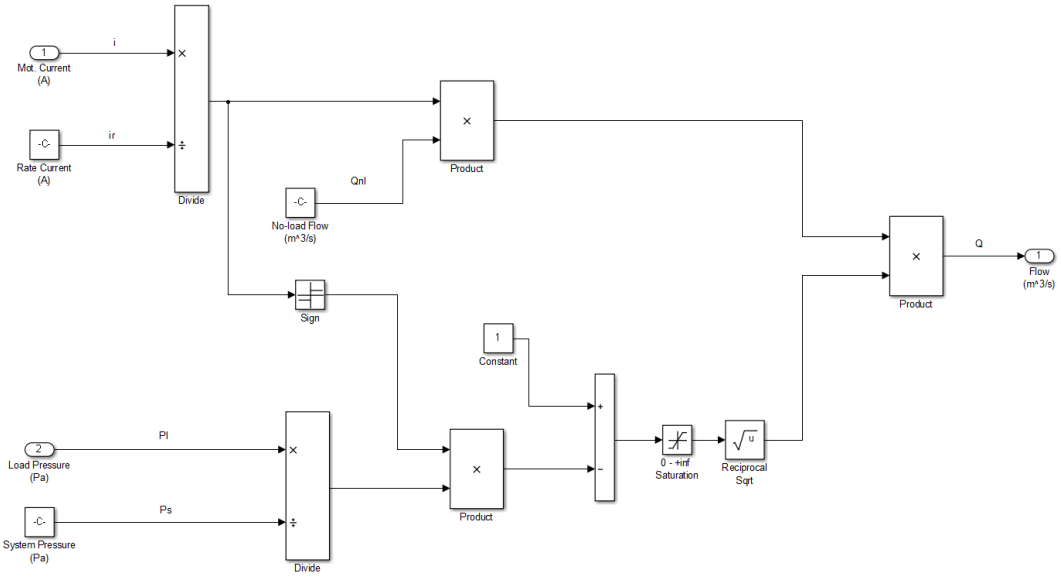

Figure 3.13: EHA — Servo-valve and cylinder model scheme — Servo-valve

Hydraulic cylinder description

The valve-flow runs directly in a hydraulic cylinder, which is one of the most common hydraulic actuator. A double-acting piston cylinder is a particular type of hydraulic cylinder, composed of a rod and a central annulus, which is easier to model, compared to other cylinder types. The central annulus divides the cylinder in two separated chambers. The rod is able to move in each of the two directions. For this reason, this device is called "double-acting cylinder", due to its capability to provide forces both in pulling the load and in pushing it back. The valve, which is upstream, allows the fluid to flow into the cylinder and move the piston. The control of this flow into the two chambers determines the direction of the movement. Few different seals are incorporated in the device in order to minimise leakage. A simplified cross-section model is shown in Figure 3.14.

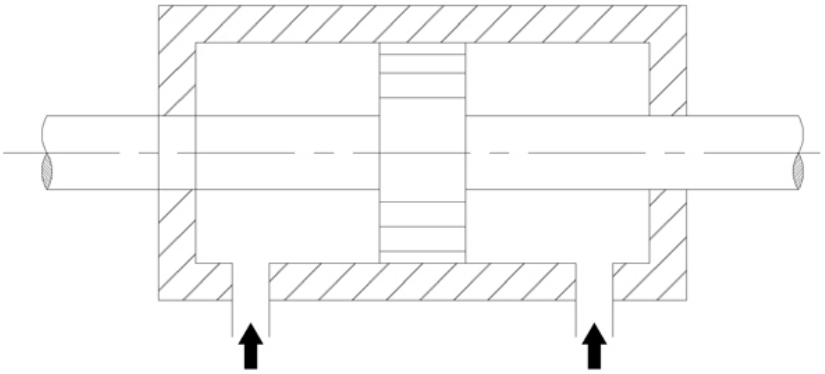

Figure 3.14: Typical double-acting hydraulic piston cylinder scheme [17]

The equation describing the behaviour of this device is a simple fluid conservation and is reported below:

$$Q = A_c \frac{dx}{dt} + \frac{V}{2\beta} \frac{dP}{dt} \tag{3.21}$$

where Q is the average flow into the actuator and P is the pressure difference on the piston of the actuator, A_c is the cylinder area, V is the cylinder volume, β is the bulk modulus and x is the piston displacement. From this equation it is possible to evaluate the pressure and so, multiplying by the cylinder area, the force given by the piston to the load.

Figure 3.15 depicts the hydraulic model of the cylinder, where the inputs are the piston velocity (m/s) from the mechanical linkage, which will be discussed later, and the valve-flow (m^3/s) from the servo-valve model. The outputs are the piston force (N) and the load pressure (Pa), which is used in the servo-valve model.

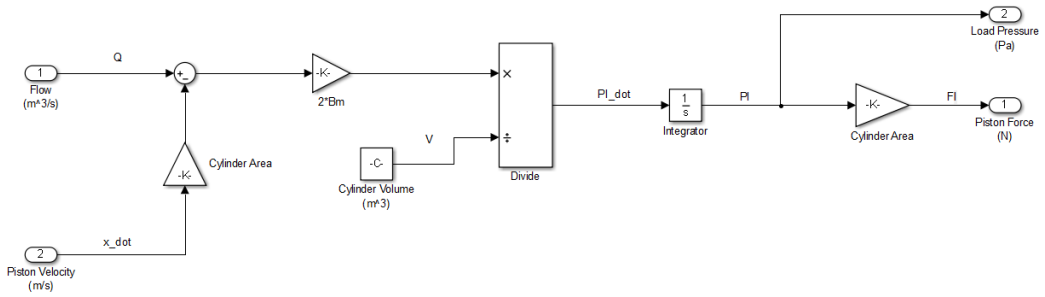

Figure 3.15: EHA — Servo-valve and cylinder model scheme — Cylinder

3.3.2 Parameters

The components chosen for this simulation are listed in Table 3.6. The parameters have been taken directly from the manufacturer's datasheets. Where these were not available,

estimation based on the performance of similar components or a simplified computation has been done. These parameters are marked with an asterisk.

Type	**Manufacturer**	**Part No.**
Flow control servo-valve	Moog	760 series
Hydraulic Cylinder	Bosh Rexroth	CGH1-MS2

Table 3.6: EHA — Servo-valve and cylinder component list [18][19]

The two components were chosen by making some considerations. Different manufacturers were considered, but the choice was made selecting the type, which had the characteristics needed in this simulation. The parameters chosen from datasheet are listed below.

Parameter	**Symbol**	**Magnitude**	**Units**
Motor armature inductance	L_a	0.59	H
Motor armature resistance	R_a	100	Ω
Motor rated current	i_r	15	mA
Servo-Valve rated flow	Q_r	2.5	gpm
Servo-Valve system pressure	P_s	3000	psi
Fluid bulk modulus	β	$1.7 * 10^9$	Kg/m^2
Cylinder area	A_c	34.36	cm^2
Cylinder volume*	V	0.0021	m^3
Piston length	L_p	0.6	m
Cylinder mass*	m_p	61.96	Kg
Piston viscous damping*	F_{v0}	1200	N*s/m

Table 3.7: EHA — Servo-valve and cylinder parameters [18][19]

One of the criteria used to select the parameters for this simulation was the profile expected from the system. For instance, the piston length was chosen in order to provide a linear displacement to the rack which allows the rails to go from one position to the other. The rated flow allows the whole system to have a time response of about two seconds, which is the time expected for a REPOINT switch.[6]

The geometric dimensions of this actuator are listed in the following table. Here the power pack is not taken into account.

Parameter	length x width x height	Units
Servo-valve	97.3 x 96 x 72.4	mm
Cylinder	1664 x 220 x 149	mm
Total dimensions	1664 x 220 x 221.4	mm

Table 3.8: EHA — Servo-valve and cylinder dimensions [18][19]

Concerning the final comparison, another element of a common EHA scheme has to be investigated in order to have a better result. This is the supply pressure power pack. Three solutions are identified, one is for a little switch. It consists of a small supply pressure system, which ensures the operation of one single switch. The second one, which is bigger, is able to provide power for more than one switch. The third one, bigger than the previous one, provides power for a larger number of switches.
In the following table the mains parameters of these three power packs are showed.

Type	Manufacturer	Part No.
Compact Power Units	HYDAC	CO1 HB12T-12.0-230-03
Power Unit	HAGGLUNDS	PEC 202
Power Unit	HAGGLUNDS	PEC 302

Table 3.9: EHA — Power packs component list [20][21]

In Table 3.10 are listed the main parameters for the Compact Power Unit of HYDAC.

Parameter	Magnitude	Units
Flow-rate	12.0	l/min
Max. motor power output	3	kW
Max. hydraulic pressure	230	bar

Table 3.10: EHA — CO Compact Power Unit parameters [20]

For the PEC 202:

Parameter	Magnitude	Units
Flow-rate	337	l/min
Max. motor power output	90	kW
Max. hydraulic pressure	350	bar

Table 3.11: EHA — PEC 202 parameters [21]

For the PEC 302:

Parameter	Magnitude	Units
Flow-rate	737	l/min
Max. motor power output	315	kW
Max. hydraulic pressure	350	bar

Table 3.12: EHA — PEC 302 parameters [21]

Furthermore, geometric dimensions are reported in Table 3.13.

Parameter	length x width x height	Units
CO1	841 x 120 x 215	mm
PAC 202	1500 x 1000 x 2320	mm
PAC 302	1670 x 1250 x 2600	mm

Table 3.13: EHA — Power packs dimensions [20][21]

Linearisation

This model is not linear, as discussed in the servo-valve and hydraulic cylinder section. In some cases, it could be better to have a linearised system. This is the reason for making a linearisation. Looking at the whole system, the only element that presents strong non-linearities is the servo-valve. All other components of the actuator are described by linear relationship. In literature a linear relationship between the flow-rate, current and pressure may be found. The equation is reported below [15].

$$Q = K_q I - K_l p \tag{3.22}$$

where Q is the flow-rate of the valve, I is the command current, p is the pressure drop among the supply pressure and the load one, K_q and K_l are the flow-current gain and the flow-pressure gain respectively.
These last parameters are the two have to be estimated in order to linearise the valve. The flow-current gain is evaluated giving a ramp input to the non-linearised valve and taking the flow-rate as an output. In addition to this, a fixed load pressure may be adopted. The choice is made by looking at the non-linear open loop load pressure characteristic. The selected value is about 4.7 10^6 Pa, which is located in the medium of the characteristic.
The resulting plot is a line. By evaluating the slope of that curve, an estimation of the flow-current gain is done. Concerning the flow-pressure gain, the approach is similar. A fixed current input is given, equal to the maximum value admissible by the motor: 15 mA. After this, the next step is to see the characteristic of flow-rate with respect of the pressure drop ($P_s - P_l$). Starting from the resulting plot, an operating point is selected

by looking at medium flow-rate values of the non-linear system. The value of flow-rate selected for this estimation is 1.2 10^{-4}m^3/s.
By measuring the slope of the profile in that operational point, the flow-pressure gain is estimated.
After this first estimation, these gains are properly tuned by comparing the deflections of the linear and the non-linear model. The final values estimated after this tuning are reported in Table 3.14.

Parameter	**Symbol**	**Value**	**Unit**
Flow-current	K_q	8.3 10^{-3}	$m^3/(\text{A s})$
Flow-pressure	K_l	5.786 10^{-12}	$m^5/(\text{N s})$

Table 3.14: EHA — Linearisation coefficients

3.4 EHA mechanical linkage

The way to transfer the movement from the electro-hydraulic actuator to the cam and the rails adopted here is simply made using a rack and pinion assembly, as the EA linkage. Nevertheless, the piston is directly attached to the rack and moves it back and forth. The cam pinions are spun by this movement without any other mechanical element.
The proposed scheme can be seen in Figure 3.9.

3.4.1 Model

The equation of motion, which describes this linkage, is a simple force balance.

$$F_p - M_{rp}\frac{d^2x}{dt^2} - B_{rp}\frac{dx}{dt} = \frac{T_h}{R_h} \tag{3.23}$$

where F_p is the force provided by the hydraulic piston, M_{rp} and B_{rp} are the lumped mass and friction of the piston and the rack, T_h is the cam torque, R_h is the cam pinion radius and x is the position displacement of the rack.
The lumped mass of the piston and the rack is simply the sum of the rack and piston mass. In the same way, the lumped friction component can be computed. In order not to overshoot the speed limits of the piston, a maximum velocity value has been considered within the model. The torque exerted by the cam pinions is a function of their torsional stiffness:

$$T_h = k_c\left(\frac{x}{R_h} - \theta_c\right) \tag{3.24}$$

where θ_c is the angle of the cam pinion and k_c is the cam pinion torsional stiffness. The model structure is shown in Figure 3.16, where the piston force (N) from the hydraulic

cylinder model and the cam velocity (rad/s) are the model inputs, instead of the piston velocity (m/s), entering the cylinder model, rack position (m) and cam pinion torque (N·m), which are the outputs.

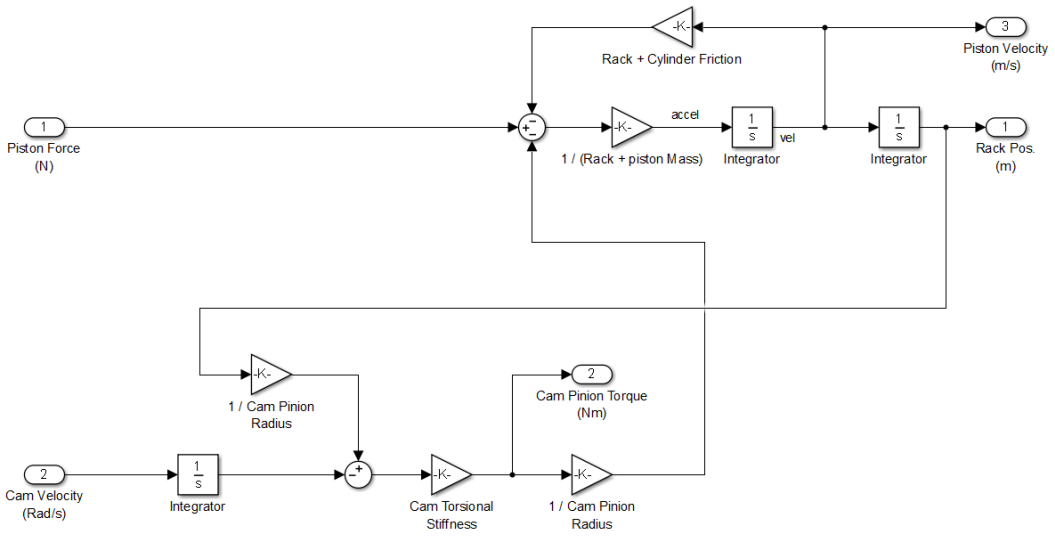

Figure 3.16: EHA — Rack and pinion model scheme

3.4.2 Parameters

As in the electro-mechanical actuator, all the parameters of this mechanical linkage are taken from manufacturers' datasheets. All other parameters are estimated starting from performances of similar components. The estimates are marked with an asterisk.

Type	**Manufacturer**	**Part No.**
Steel Pinion Gear and Shaft	HPC Gears	ST4-15
Steel Spur Rack	HPC Gears	CR4

Table 3.15: EHA — Rack and pinion components list [11][12]

Parameters	**Symbol**	**Magnitude**	**Units**
Rack mass	M_{ma}	14.3	Kg
Rack friction coefficient*	B_{ma}	0	N/ms^{-1}
Hopper pinion radius	R_h	0.03	m
Hopper torsional stiffness*	k_c	40	Nm/Arc-min

Table 3.16: EHA — Rack and pinion parameters [11][12]

3.5 Torque motor

The last actuator taken into account is a torque motor. The peculiarity of this device is to provide huge values of torque with low speed. This is obtained by using high-strength permanent magnet stators, which are able to provide an almost constant and uniform magnetic field. The proposed actuator is depicted in Figure 3.17.

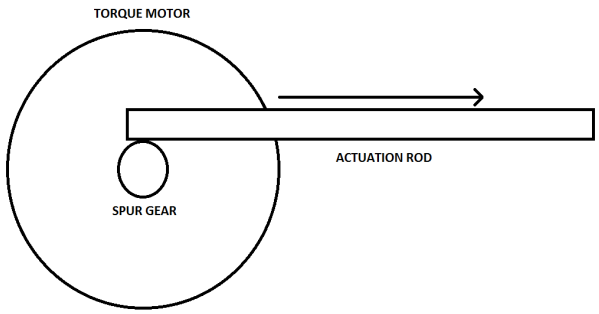

Figure 3.17: Proposed scheme of the torque motor actuator

A top level model of this actuator is shown in Figure 3.18. Two input are present in this model, motor voltage (V) and a load torque (N·m) coming from the mechanical linkage model. The outputs are the motor velocity (rad/s), the motor current (A) and the motor power input and output (W).

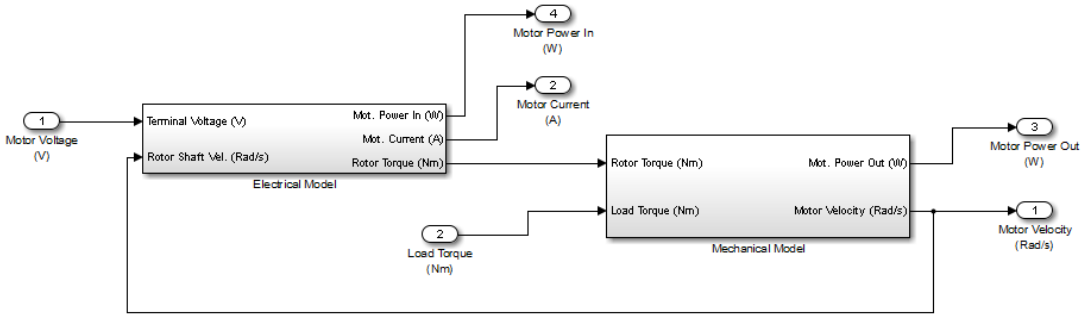

Figure 3.18: TMA — Torque motor model scheme — Top level

3.5.1 Model

Electric motor

The principle of this actuator is all based on this particular electric motor. The torque motor is, essentially, a brushless DC motor, with particular characteristics. Due to the materials and the way it is built, high values of back electromotive force and torque coefficients are obtained.
The equations describing the behaviour of this motor are the typical ones:

$$\begin{cases} V = R_a \cdot I + L_a \cdot \dfrac{dI}{dt} + E \\ E = k_e \cdot \Omega_m \\ T_m = k_t \cdot I \end{cases} \tag{3.25}$$

where V is the armature motor voltage, R_a is the armature resistance, I is the armature current, L_a is the armature inductance, E is the back emf, k_e is the back emf constant, Ω_m is the angular position of the rotor, T_m is the motor torque, and k_t is the motor torque constant.
At variance with the EHA model, here the back emf component is considered, because the other parameters of the torque motor make this value not negligible. The torque motor taken into account in this work has very big dimensions, thus very high torque.
The actuator electrical model is shown in Figure 3.19, using the motor voltage (V) and the rotor shaft velocity (rad/s) from the actuator mechanical model, as inputs and motor current (A), motor power input (W) and rotor torque (N·m) as outputs.

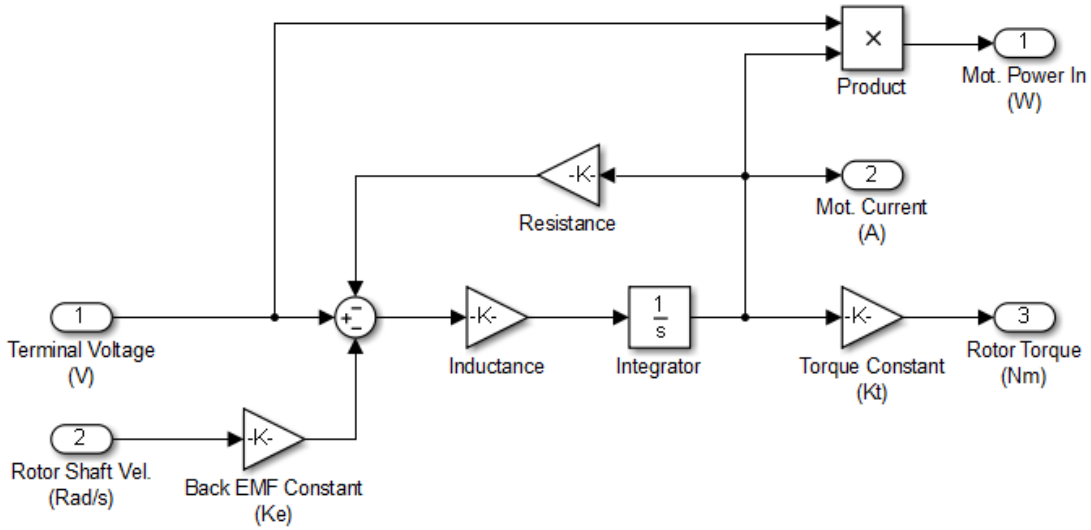

Figure 3.19: TMA — Torque motor model scheme — Electrical model

Then, a simple torque balance describes the mechanical output of this motor.

$$T_m - T_l = J_m \frac{d^2\theta}{dt^2} + D_m \frac{d\theta}{dt} \tag{3.26}$$

where T_l is the load torque D_m is the motor friction constant. The mechanical model structure is reported in Figure 3.20.

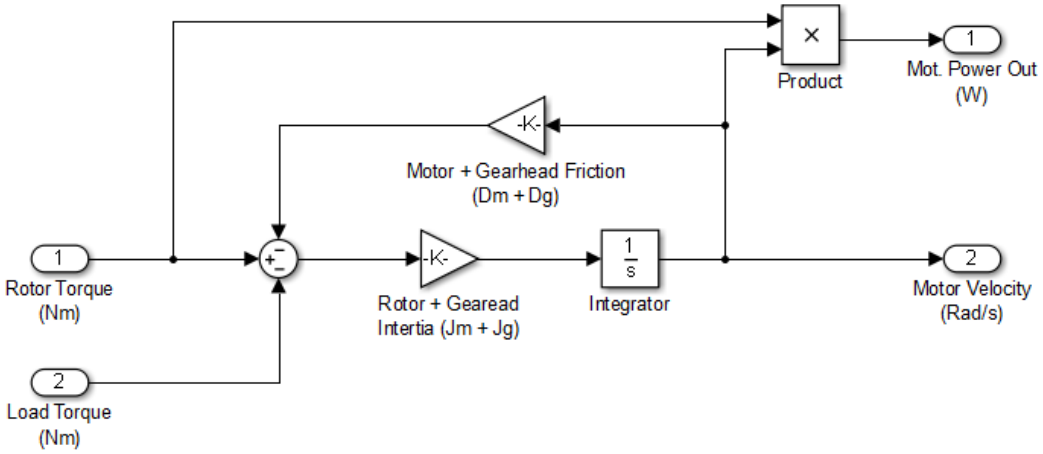

Figure 3.20: TMA — Torque motor model scheme — Mechanical model

In this figure rotor torque (N·m) from the electrical model and the load torque (in N·m) from the mechanical linkage are the inputs; the motor power output (W) and the motor velocity (rad/s) are the outputs.

3.5.2 Parameters

All the parameters are taken from manufacturers' datasheets.

Type	**Manufacturer**	**Part No.**
Brushless DC Torque Motor	ETEL	TMB0760-070 3VCN

Table 3.17: TMA — Motor component list [22]

Parameter	Symbol	Magnitude	Units
Motor armature inductance	L_a	36.6	mH
Motor armature resistance	R_a	2.99	Ω
Motor back EMF constant	K_e	50.2	$V_{rms}/rads^{-1}$
Motor torque constant	K_t	86.7	Nm/A_{rms}
Motor viscous damping*	D_m	9.49	Nm/k_{rpm}
Motor inertia	J_m	2.30	Kg m^2
Motor peak torque	T_p	5240	Nm
Motor continuous torque	T_c	1320	Nm
Motor max. continuous power dissipation	P_c	1560	W
Motor peak current	I_p	115	A_{rms}
Motor continuous current	I_s	15.6	A_{rms}

Table 3.18: TMA — Motor parameters [22]

The geometric dimensions of this particular torque motor are reported in Table 3.19.

Parameter	length x width x height	Units
Torque motor	795 x 795 x 150	mm

Table 3.19: TMA — Motor dimensions [22]

3.6 TMA mechanical linkage

As the previous actuators, the general idea of how to link the cams to the actuator is the same. This means a rack and pinions assembly, as explained before. The only difference is the way the rack is connected to the motor. This is made through a spur gear, directly screwed on the rotor of the torque motor. This mechanical linkage can be seen in Figure 3.17.

3.6.1 Model

The model of this linkage is similar to the previous ones.
The spur gear spins at the same velocity of the rotor. The output gear torque is a function of velocities and a torsional stiffness.

$$T_g = k_g \left(\theta_g - \frac{x}{R_g} \right) \tag{3.27}$$

where T_g is the spur gear torque, θ_g is the rotational spur gear velocity, R_g is the spur gear radius, x is the displacement of the rack, and k_g is the torsional stiffness of the spur gear.
The angle θ_g of the spur gear is equal to the angle θ calculated before, since the gear is

directly screwed on the rotor surface.
The cam pinions behaviour is described by a similar relationship to the other actuators, and is reported, here, for simplicity.

$$T_h = k_c \left(\frac{x}{R_h} - \theta_c \right) \tag{3.28}$$

where θ_c is the angle of the cam pinion and k_c is the cam pinion torsional stiffness.
The final equation of motion for the rack assembly is:

$$\frac{T_g}{R_g} - \frac{T_h}{R_h} = M_{ma} \frac{d^2x}{dt^2} + B_{ma} \frac{dx}{dt} \tag{3.29}$$

where T_h is the torque from the cam pinion, B_{ma} is the rack assembly friction coefficient, M_{ma} is the mass of the rack assembly.
In Figure 3.21 the model structure can be seen.

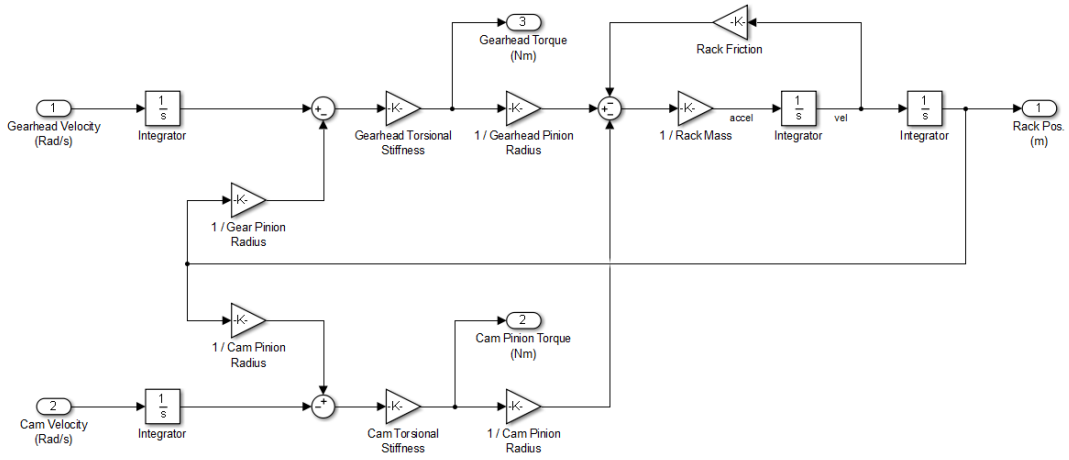

Figure 3.21: TMA — Rack and pinion model scheme

Here, the inputs are the spur gear velocity (rad/s) from the actuator mechanical model, and the cam pinion velocity (rad/s) from the cams and hopper model. The outputs, instead, are the spur gear and cam pinion torque(N·m), and the rack position (m).

3.6.2 Parameters

The parameters are selected looking directly to manufacturers' datasheets. The missing parameters are, instead, evaluated by simple mechanical laws or by looking to similar components. The estimates are marked with an asterisk.

Type	Manufacturer	Part No.
Steel Pinion Gear and Shaft	HPC Gears	ST4-15
Steel Spur Rack	HPC Gears	CR4
Heavy Duty Steel Spur Gear	HPC Gears	

Table 3.20: TMA — Rack and pinion components list [11][12][13]

Parameters	Symbol	Magnitude	Units
Rack mass	M_{ma}	14.3	Kg
Rack friction coefficient*	B_{ma}	0	N/ms^{-1}
Gearhead pinion radius	R_g	0.02	m
Hopper pinion radius	R_h	0.03	m
Gearhead torsional stiffness*	k_g	37.3	Nm/Arc-min
Hopper torsional stiffness*	k_c	40	Nm/Arc-min

Table 3.21: TMA — Rack and pinion parameters [11][12][13]

Chapter 4

Cams and Rail Modelling

The aim of each actuator considered in this work is to provide a linear backward and forward movement to a rack. This mechanism is directly attached to the main innovative part of the REPOINT switch, i.e., the system actuating the switch rails. Cam pinions convert the linear motion of the rack into a rotation. Four cams are spun in this way, providing the force needed to bend the bearers. All the cams are built underneath a hopper on which the switch rails are fixed. Figure 4.1 shows this part of the system. This system allows to move the rail pair from one position to the other easily and safely.

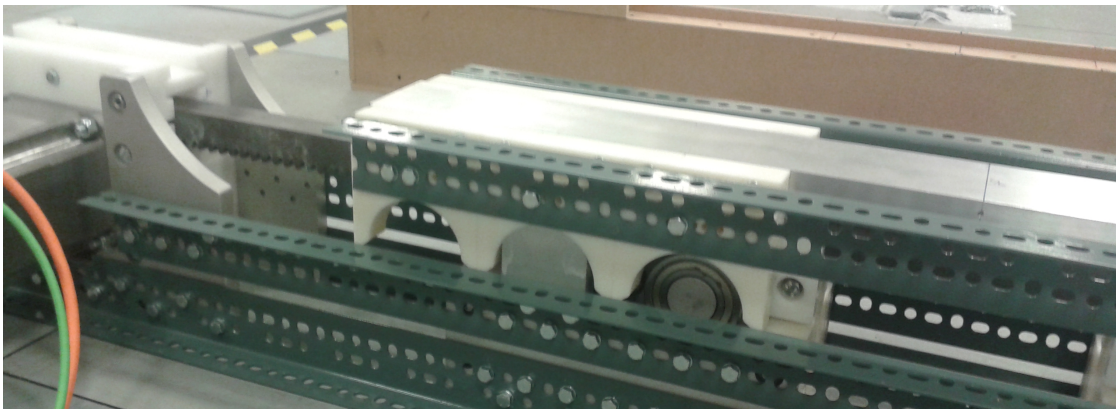

Figure 4.1: REPOINT laboratory demonstrator cams and hopper assembly, illustration courtesy Loughborough University

4.1 Cams and Hopper Model

The four cams and hopper model is characterised by considering simple motion equations. The idea is to balance the mass of the hopper across four identical cams.
The aim of the desired design is to bend the rails in the vertical plane to move them between the positions. For their nature they are resistant to bending in this plane. That's

why for the REPOINT design, a particular profile of the cams is selected, to guarantee the follower (the hopper) to move through a half circle path, as explained in Chapter 2. In Figure 4.2 is depicted a scheme for this system.

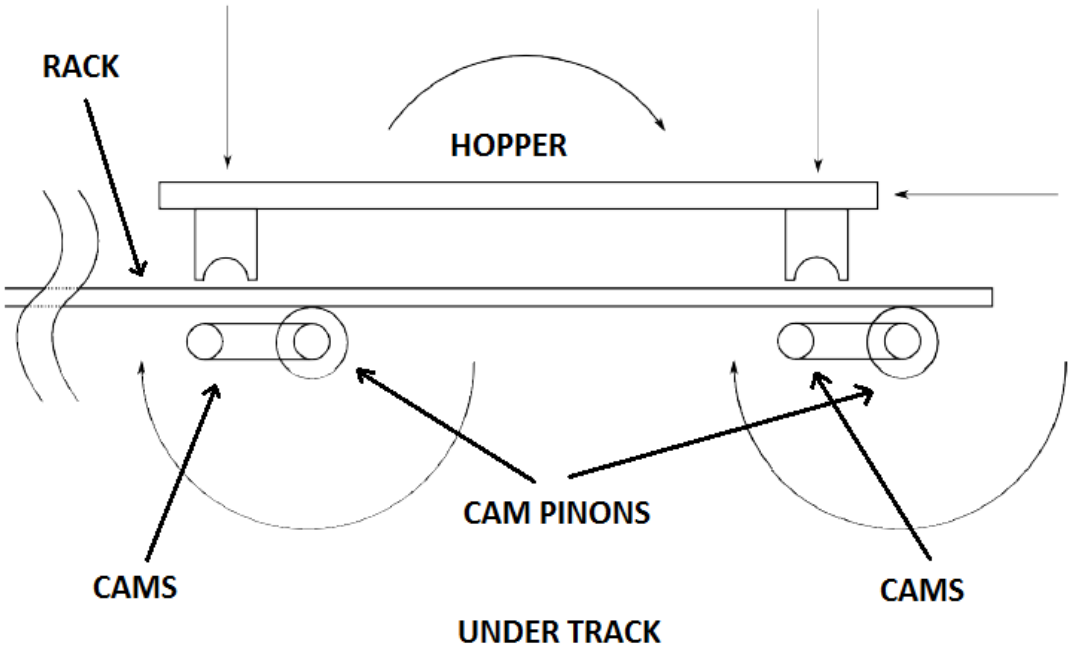

Figure 4.2: Proposed cams and hopper assembly scheme

4.1.1 Model

The cams and hopper can be modelled according to a torque balance across all the parts of this section. The torque from both cams is found by solving the following equation:

$$T_h = R_h \left[\cos(\theta_c)(P_v + m_h g) + \sin(\theta_c)P_h\right] + J_h \frac{d^2\theta_c}{dt^2} + \frac{d\theta_c}{dt} B_h \tag{4.1}$$

where P_v is the vertical force component on the hopper, P_h is the horizontal force component on the hopper, m_h is the mass of the hopper, g is gravity acceleration, J_h is the cams and hopper inertia, θ_c is the angular position of the cams, and B_h is the friction coefficient between the cams and the hopper. The model structure is presented in Figure 4.3.

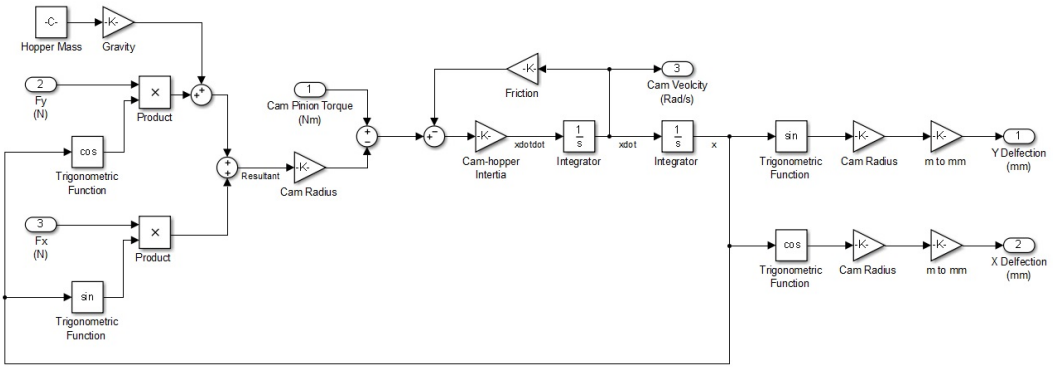

Figure 4.3: Cams and hopper model scheme

In this figure can be seen the input variables, which are the cam pinion torque (N·m) coming from the mechanical linkage model of each actuator design, and the vertical and lateral reaction forces (N) coming from the switch rail model explained later. The outputs are the cams velocity (rad/s), which is given to the transmission model of each actuator, and the vertical and lateral deflections of the bearers (mm) needed for evaluating the reaction forces.
As can be noted, this portion represents the non-linear part of the model of a REPOINT switch, because of the presence of the reaction forces of the switch rails.

4.1.2 Parameters

The parameters of these components are peculiar compared to all the others. The cams and the hopper are custom made parts, therefore many parameters have been calculated from basic mechanics and physics formulas.

Parameter	**Symbol**	**Magnitude**	**Units**
Hopper mass	m_h	25	Kg
Cam-hopper inertia	J_h	0.003	Kg-m^2
Cam-hopper friction coefficient	B_h	4	Nm/$rads^{-1}$
Cam radius	R_c	0.08	m

Table 4.1: Cams and hopper parameters [10]

4.2 Rail Pair Model

Looking at the whole switch, it is reasonable to think that the most significant load will be the one that comes from the bending of the rail pair. This particular load interacts

with the cam and hopper system by providing a reaction force on each actuator bearer.

In order to calculate these reaction forces the beam deflections have to be evaluated. In the literature many methods can be used to do this. McCauley's is one of those methods, which allows to represent the bending moment along a beam in an easy and compact way, in particular when more than one force is applied on the beam [23]. In the final installation of the REPOINT switch, where three actuator bearers are present, this method becomes useful. In the current work, however, a simplified model is considered. It describes the behaviour of the laboratory demonstrator. The laboratory demonstrator is composed of one single bearer, as explained in Chapter 2. For this reason, the model illustrated here considers only one vertical and lateral forces coming from the actuator bearer. A simplified diagram of the vertical forces and the moments acting on the beam are shown in Figure 4.4. The bending of the switch rail in the horizontal direction may be represented in an equivalent way, and, for this purpose, the calculations are not reported in this work.

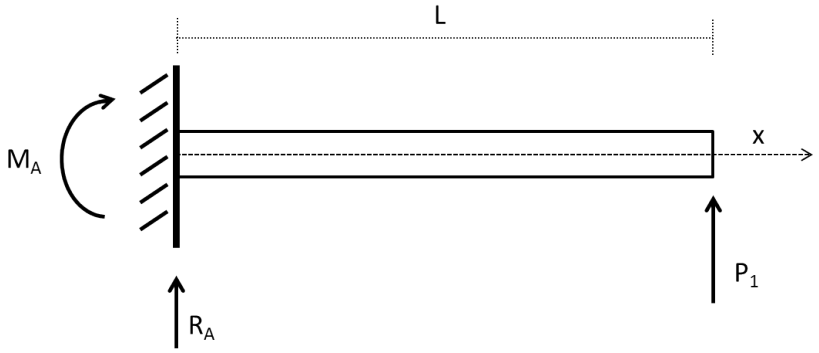

Figure 4.4: A diagram of the moments and the forces present on the considered model

Here, M_A and R_A are the moment reaction and the vertical reaction at the anchor point, x is the distance along the rail from the anchor point, P_1 is the vertical force from the actuator bearer, and L is the total length of the rail from the anchor point. The weights of the fixings are not taken into account here, because they have already been lumped in the 'hopper mass'(m_h) of Table 4.1, and, in addition to this approximation, it is assumed to work with a constant cross-sectional beam. Furthermore, considering the ease of this simplified model, a more standard approach may be used to calculate the reaction forces. Starting from this model, one may build another diagram representing the moments and the forces present on the beam, cut in a generic point x of its length, as depicted in Figure 4.5.

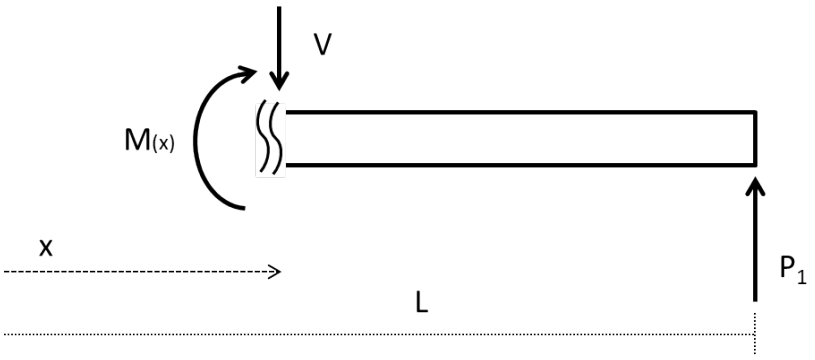

Figure 4.5: A diagram of the moments and the forces present on a part of the beam

Afterwards, a balance of all the moments acting on this section of the beam is done, obtaining:

$$M(x) = P(L - x) \tag{4.2}$$

Now, by recalling Euler-Bernoulli theory, this relationship between the bending moment and the vertical deflection may be written:

$$\frac{M(x)}{EI} = \frac{d^2 u_y}{dx^2} \tag{4.3}$$

where u_y is the vertical deflection of the beam, E and I are the elastic modulus and the area moment of inertia of the beam.
By substituting Eq.4.2 in Eq.4.3, and, then, by integrating two times the resulting equation, the expression for the deflection along the beam is:

$$EIu_y = -P_1 \left(\frac{x^3}{6} - \frac{Lx^2}{2} \right) + C_1 x + C_2 \tag{4.4}$$

where C_1 and C_2 are the two integrations constants. This means that two boundary conditions are needed in order to obtain the final result. These conditions are:

$$u_y(0) = 0 \tag{4.5}$$

$$u'_y(0) = 0 \tag{4.6}$$

Therefore:

$$C_2 = 0 \tag{4.7}$$

$$C_1 = 0 \tag{4.8}$$

The final equation for the vertical deflection is:

$$u_y = -\frac{P_1}{EI}\left(\frac{x^3}{6} - \frac{Lx^2}{2}\right) \tag{4.9}$$

Finally, rearranging Eq.4.9, the expression for the vertical force from the actuator bearer is obtained. As already explained before, a same procedure can be made for the lateral force. The final equations, which are implemented in the model, are:

$$P_{1UP} = -\frac{u_y EI}{\frac{x^3}{6} - \frac{Lx^2}{2}}$$

$$P_{1LAT} = -\frac{u_x EI}{\frac{x^3}{6} - \frac{Lx^2}{2}} \tag{4.10}$$

where P_{1UP} and P_{1LAT} are the reaction forces of the bending rail, u_y and u_x are the vertical and lateral deflections of the rail, x is the distance along the rail from the anchor point, and L is the full length of the rail.
The rail shape used in this work is a light flat bottom rails for use in mines [24], and is showed in Figure 4.6.

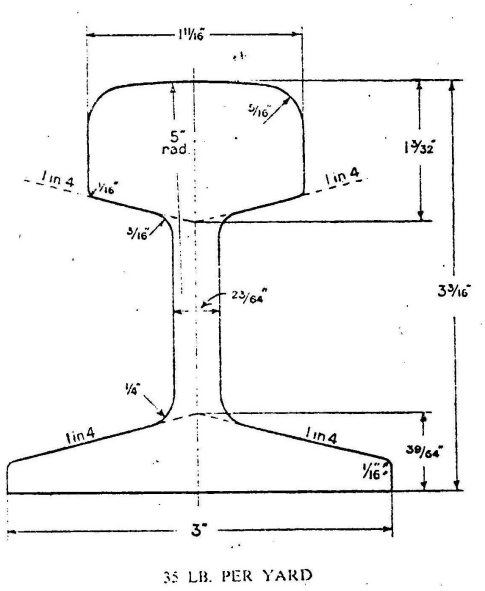

Figure 4.6: Section of the British standard light flat bottom rails for use in mines [24]

The area moment of inertia is evaluated starting from this standard section.

4.2.1 Parameters

In the following tables all the parameters used to calculate the reaction force of the rail pair are listed. Table 4.2 shows the parameters used for evaluate the vertical reaction force.

Parameter	**Symbol**	**Magnitude**	**Units**
Rail length	L	4.501	m
Deflected part of the rail	x	4.5	m
Modulus of elasticity	E	$207 \cdot 10^3$	N/mm
Geometric moment of inertia	I	$3188 \cdot 10^4$	mm^3

Table 4.2: Rail parameters — Vertical reaction force [10]

Table 4.3, instead, shows the parameters for the lateral reaction force.

Parameter	**Symbol**	**Magnitude**	**Units**
Rail length	L	4.501	m
Deflected part of the rail	x	4.5	m
Modulus of elasticity	E	$207 \cdot 10^3$	N/mm
Geometric moment of inertia	I	$672 \cdot 10^4$	mm^3

Table 4.3: Rail parameters — Vertical reaction force [10]

Chapter 5

Control

In this chapter all the control designs are reported. The general idea is to use only proportional (P) or proportional and integrative (PI) controllers. This because of their facility in implementation and also because there is no reason to do something more complex considering the good results obtained with these strategies.
Nevertheless, it has to be noticed that the model of a REPOINT switch presents some non-linearities, due to the presence of the reaction forces from the switch rails, as explained in Chapter 4.
Thus, these families of controllers (i.e., P and PI) are not the best solutions from a stand point of performance and robustness, but they are suitable for this particular work, as can be seen from the later simulation results. The control system design is not really the target of this project, which is to analyse the performances of the system. For this purpose, a non-linear design will take too much time to be done. Moreover, the results obtained with these easier control designs are sufficient to make a reasonable performance comparison among the actuator solutions.
The control schemes, discussed in this Chapter, are designed with the help of the *'Control Design Tool'* of MATLAB SIMULINK®, which offers an easy way to plot frequency responses of different part of the system, by linearising the system itself. The operating point selected is different for each actuator system, because it refers to the point where the cam load torque is largest. This always represents the "worst case" situation, when the motor needs to produce the highest torque. If the designed controller is able to control the system in this "worst" situation, it is reasonable to assume that it will be able to regulate it for the rest of the cam cycle.
These assumptions were validated by looking at the simulations in the time domain of the non-linear starting systems. This approach is thought to fit the purpose of this work, since the control design is not the main task of this comparison.

In addition to these considerations, different requirements are taken into account for each actuator. Moreover, some performance elements are in common for all the models. In particular, there are the typical performance and stability constraints that come from the frequency response analysis. Typically, these values are the phase margin (PM), greater than 60°, and the gain margin(GM), greater than 6 dB [7]. These constraints can give some assurance that the closed-loop system transient resulting from the response characteristics will be acceptable. This means that by imposing these restrictions, if there are no great unusual situations, a reasonable stability margin will be provided.
However, these margins are valid only if the considered system is linear, from this the necessity to linearise the system. The way the systems were linearised was explained in the previous paragraph.
Other constraints come from a time response analysis. They are limits of rising time and general behaviour of the response.
A desirable rising time, for instance, is selected by looking to the expected REPOINT performances, already discussed in Chapter 2. In particular, it is expected that a REPOINT switch reaches its final position in about two seconds [6]. However, the following simulations are performed asking the switch rails a double movement in the same direction, that is the case of two turnouts (i.e., in this work it will called three-position turnout). This choice is made because the lateral deflection increases if the switch has to move the rails among more than two positions. A lateral deflection increment means a higher reaction force, hence the actuator has to provide more torque than the case with a single two-position turnout. If for a two-position turnout (that is the most common one, also shown in Figure 2.1) the rack displacement is about 0.0942 m, for the simulations made here the position set-point is about twice the previous value, i.e., 0.1885 m. Thus, if for the two-position turnout the movement should be completed in two seconds, for the three-position one the movement will take four seconds. Starting from this value, a desirable frequency has been chosen, which is reported in Table 5.1. Setting up the controls considering a three-position turnout, instead of the two-position one, corresponds tuning these controls in a sort of "worse case", which may provide more reliability to the system.
Concerning the general behaviour of the response, two constraints are taken into account for the position controls. They are the zero steady-state error and the absence of overshoots, and they must not be exceeded in any case. These two requirements are very important considering the safety for the entire switch. In a general turnout, indeed, the perfect matching between the switch and the stock rails is required, in order to avoid the danger of derailment, which otherwise would increase significantly. At the same time, the presence of overshoots, when the moving rails approach to the fixed ones, may cause damages. These are the reasons for imposing these constraints. One of the most common techniques to achieve this behaviour is obtaining an over-damped system.

At least, a limit voltage demand is taken into account for each actuator scheme. This limit is referred to the maximum voltage available from the power supply. In this work this value corresponds to the one accessible in the laboratory, which is 415 V.
In Table 5.1 all the constraints and all the requirements explained before are listed.

Requirement	**Value**	Units
Phase margin	60°	
Gain margin	6	dB
Position rise time	4	s
Desired frequency of position loop	1.57	rad/s
Maximum supply voltage	±415	V

Table 5.1: Control requirements and constraints

The control system adopted for each actuator is composed of three net loops: current loop, velocity loop and position loop. In particular, the current loop and the position loop are the same for each actuator scheme. The controlled variables in these loops are the motor current and the rack position. A different discussion may be done for the velocity loop. The controlled variable in this system is the rack velocity for the EHA and motor velocity for EA and TMA.
This choice is done considering the fact that all these control variables are easy to measure. For example, the motor current and velocity measurements are directly provided by the servo-drive of the motor. The rack position and velocity may be measured or evaluated with standard sensors, like encoders or accelerometers.

5.1 Electro-mechanical Actuator

The control for the EA is set up by considering the laboratory demonstrator as a starting point. In fact, the electro-mechanical actuator model considered in this work differs from the one in the laboratory only by the model of the rail pair. For this reason, the starting parameters for the controls are taken from the real plant. After this first step, a new tuning is performed in order to fit properly the desired response of the system. The rail pair model introduces some non-linearities, as explained in Chapter 4. For this reason, the parameters used in the lab demo, where the switch rails are not modelled, are not directly suitable for this control design, because of the pretty different behaviour of the complete system.

5.1.1 Requirements

A way to decide the desired parameters of a control is to define, previously, which are the constraints and profiles required for the control. The requirements consist of some limitations on the electronic components used in the lab demonstrator. In particular, it is the case of the servo-drive and the dSpace unit. These devices present some voltage limitations, which are taken into account.
All the requirements for this control are reported in Table 5.2.

Requirement	**Value**	Units
Phase margin	60°	
Gain margin	6	dB
Velocity rise time	0.07	s
Desired frequency of velocity loop	8.975	rad/s
Position rise time	4	s
Desired frequency of position loop	1.57	rad/s
Maximum supply voltage	±415	V
Maximum dSpace output voltage	±10	V

Table 5.2: EA — Control requirements

5.1.2 Design and simulation

The control design chosen for the EA consists of an outer-loop rack position P controller, an inner-loop motor velocity PI controller, and an internal inner-loop motor current P controller.
The parameters of these controllers are tuned starting from the innermost loop. The motor current proportional parameter of the controller is found in accordance with the stability margin constraints first, and then looking at the step response of the non-linear system in the time domain.
In Figure 5.1 and Figure 5.2 the frequency response and the step response of the controlled system are shown.

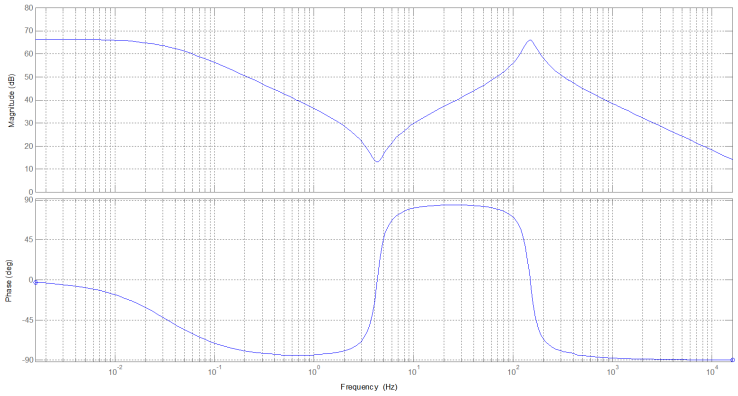

Figure 5.1: EA — Frequency response current control loop. $PM = 90$, $GM = \infty$

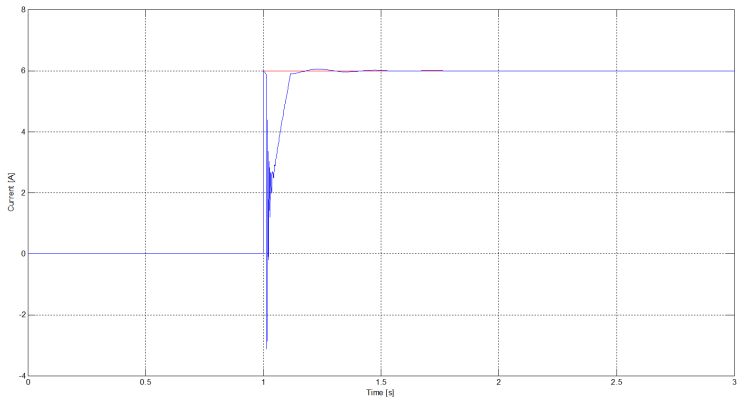

Figure 5.2: EA — Step response of the current control. The red curve is the set point, instead the blue profile is the measure variable

As shown in these pictures, all the requirements are fulfilled. Indeed, $PM = 90$ and $GM = \infty$, and there is a zero steady-state error.

The same procedure is replicated for the motor velocity PI controller. Concerning this design, another consideration has to be done. In fact, as reported in Table 5.2, another requirement needs to be considered: the dSpace output voltage. This device requires to control the voltage output of the control unit, avoiding overshoots. A common technique used to solve this problem is to implement an anti-windup scheme. Among the various scheme types of this algorithm the back-calculation one is chosen, because it is easier than others in terms of implementation. It is common use to design this control utilising the velocity rise time, which is the integral time of the considered loop, as the tracking time constant.
The results of this design in terms of frequency response and step response are reported

in Figure 5.3 and Figure 5.4.

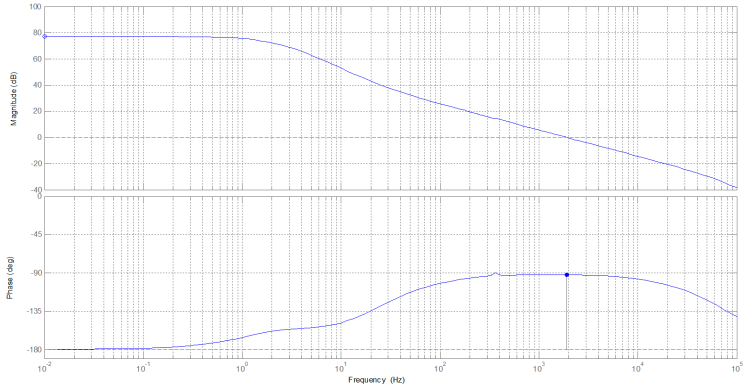

Figure 5.3: EA — Frequency response velocity control loop. $PM = 77.4$, $GM = \infty$

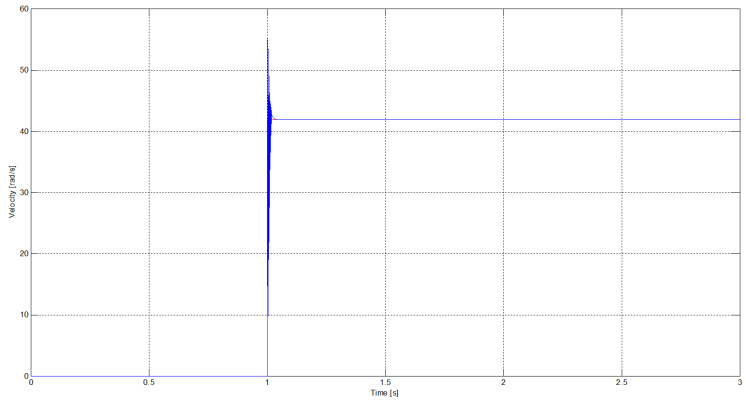

Figure 5.4: EA — Step response of the velocity control. The red curve is the set point, instead the blue profile is the measure variable

From these figures it can be inferred that the stability margins are not crossed ($PM = 77.4$, $GM = \infty$) and the set-point is reached.
The outermost position control is a proportional, and controls the rack position. The way it is tuned is the same of the current loop.
The frequency response and the step response results are shown in Figure 5.5 and Figure 5.6.

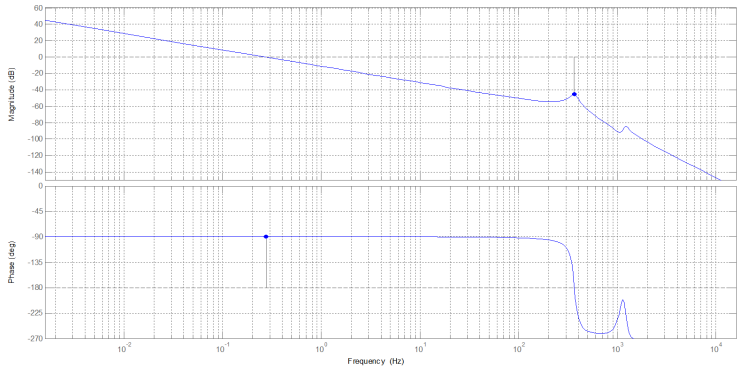

Figure 5.5: EA — Frequency response position control loop. $PM = 90$, $GM = 45.3dB$

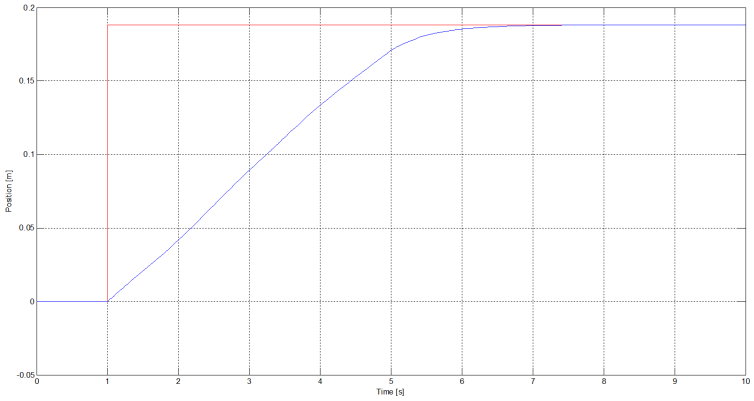

Figure 5.6: EA — Step response of the position control. The red curve is the set point, instead the blue profile is the measure variable

These final plots show that all the requirements are fulfilled. Indeed, $PM = 90$, $GM = 45.3$ dB, there are no overshoots and the steady-state error is zero.
Finally, in Table 5.3, all the control parameters used in these three nets are listed.

Parameters	**Symbol**	**Value**
Current loop proportional gain	K_{pc}	4000
Velocity loop proportional gain	K_{pv}	5
Velocity loop integral time constant	τ_{iv}	0.007 s
Position loop proportional gain	K_{pp}	3000

Table 5.3: EA — Control parameters

5.2 Electro-hydraulic Actuator

As for the EA model, also for the EHA a three net control design is adopted. However, here the actuator model is non-linear, and this will complicate the design of the control. For this reason, the system is controlled by considering the linearised actuator model discussed in Chapter 3.

5.2.1 Requirements

The requirements for this control are based on times and frequency responses, and manufacturer's specifications. This type of actuator presents more physical limitations than the others, since all its components are more complex with respect to the ones of other actuators (e.g., servo-valve and hydraulic cylinder are more complex systems compared to BLDC or Torque motors). In particular, it has limitations regarding the motor current and the maximum piston velocity. All these limits are taken from the producer's datasheets.
The maximum current accepted by the torque motor of the servo-valve is in the order of some dozen of milliamperes. This limit must not be exceeded to avoid any damages of the motor; for this reason is necessary to keep away from this condition.
Another important limit of the electro-hydraulic actuator is the maximum velocity of the motion of the piston inside the cylinder. It is necessary to not overcome this velocity, because the actuator is not able to provide that velocity and could even be damaged.
Lastly, it may be noticed that the rise times selected for this control were found out by looking at the simulation plots of the open-loop system.
All these requirements are summarised in Table 5.4.

Requirement	**Value**	Units
Phase margin	60 °	
Gain margin	6	dB
Velocity rise time	0.75	s
Desired frequency of velocity loop	8.337	rad/s
Maximum supply voltage	±415	V
Maximum motor current	±15	mA
Maximum piston velocity	0.508	m/s

Table 5.4: EHA — Control requirements

5.2.2 Design and simulation

The three loops chosen in this work are an inner-loop current control (P), a middle-loop velocity control (PI) and a position control loop (P) outside the previous one. This

scheme allows to reach all the tasks and comply with all the constraints. The velocity used for this control is the piston velocity of the cylinder, and the position control variable taken in consideration is the displacement of the rack.

The innermost loop is again the first being designed. A P controller is tuned in order to control the motor current.
First of all, the parameter is selected so that the stability margins are not exceeded. Then, by looking to a step response in the time domain, the final tuning is made.
In Figure 5.7 and 5.8 the frequency response and the step response in the time domain of the system are shown.

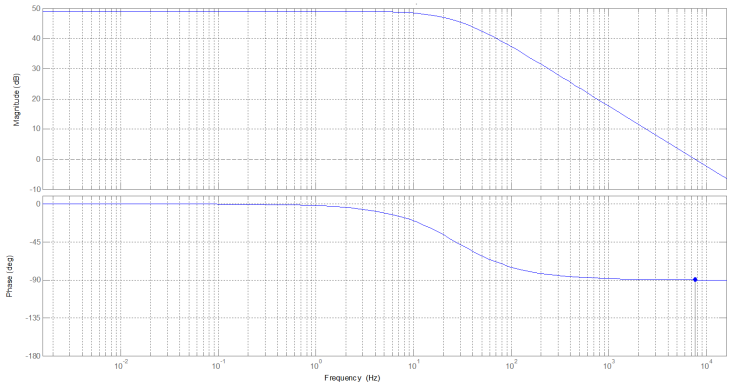

Figure 5.7: EHA — Frequency response current control loop. $PM = 90.2$, $GM = \infty$

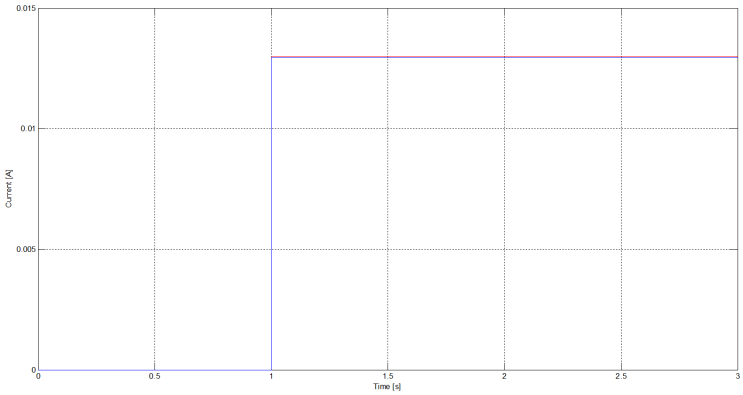

Figure 5.8: EHA — Step response of the current control. The red curve is the set point, instead the blue profile is the measure variable

In these first pictures it can be seen that all the stability margins are fulfilled ($PM = 90.2$, $GM = \infty$) and the current set-point is reached.
Once the inner control is set up, the next one can be tuned. The procedure to choose the

parameters of the PI controller is similar to the inner-loop. Looking at the responses of the system to this control, however, a problem comes out. The current reached from the system overcomes the current constraint of the torque motor. In order to fix this problem an anti-windup scheme is implemented. The scheme set up in this project is the back-calculation anti-windup scheme. The back-calculation gain used is the reciprocal of the time constant of the integral part.
Finally, another tuning is made for the proportional and the integral part in order to fit better the time response to the desired shape.
The results are shown in Figure 5.9 and Figure 5.10.

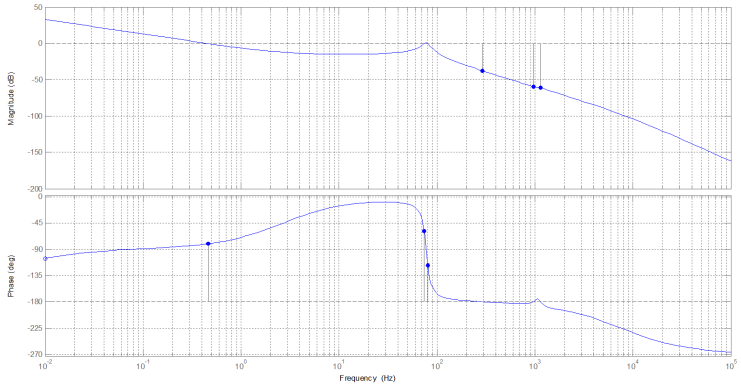

Figure 5.9: EHA — Frequency response velocity control loop. $PM = 62.1$, $GM = 37.7$

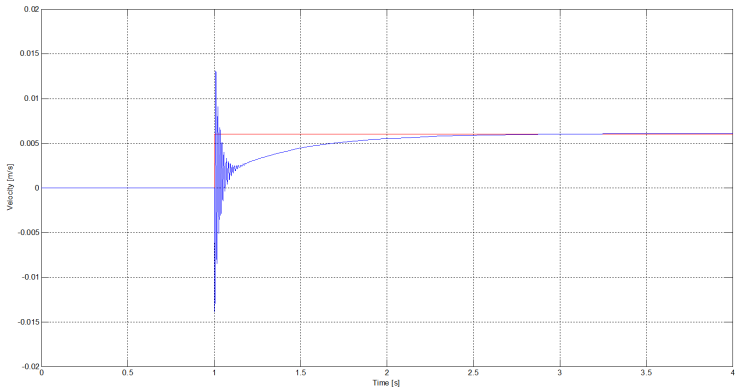

Figure 5.10: EHA — Step response of the velocity control. The red curve is the set point, instead the blue profile is the measure variable

The last two figures show that the phase and the gain margin are respected ($PM = 62.1$, $GM = 37.7$), and, also, that the set-point is reasonably reached.
Outside the velocity loop, a position proportional control is designed, so that it is possible

to move the switch rail between positions. The design steps are the same of the current control.
In Figure 5.11 and Figure 5.12 the two responses are plotted.

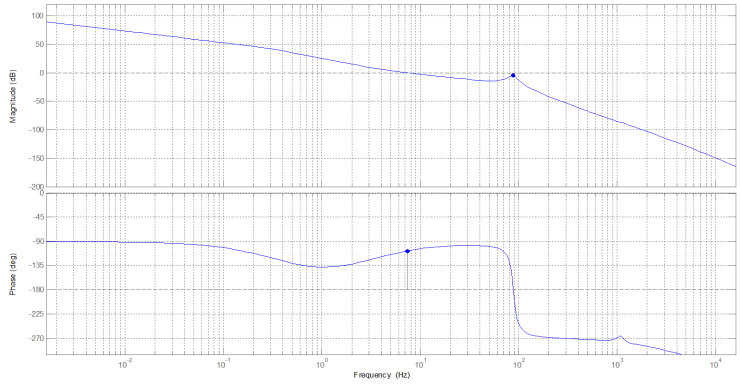

Figure 5.11: EHA — Frequency response position control loop. $PM = 64.4$, $GM = 9.08dB$

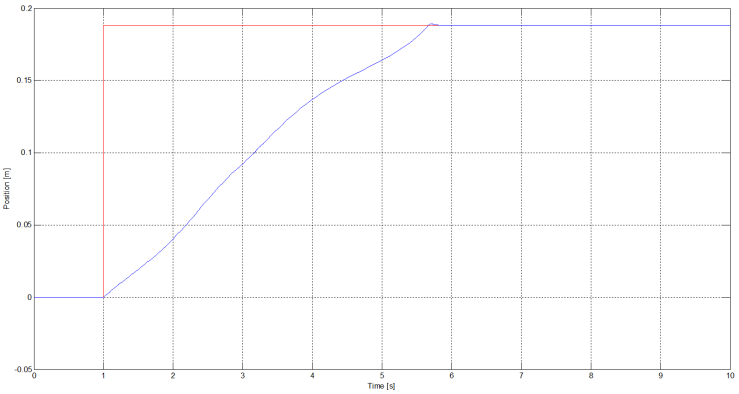

Figure 5.12: EHA — Step response of the position control. The red curve is the set point, instead the blue profile is the measure variable

In these final figures one can see that this control reaches all the requirements, like stability margins ($PM = 64.4$, $GM = 9.08dB$), not relevant overshoots and zero steady-state error.

In Table 5.5 are listed all the parameters of the electro-hydraulic actuator controllers.

Parameters	Symbol	Value
Current loop proportional gain	K_{pc}	28000
Velocity loop proportional gain	K_{pv}	0.055
Velocity loop integral time constant	τ_{iv}	0,0596 s
Position loop proportional gain	K_{pp}	351

Table 5.5: EHA — Control parameters

5.3 Torque motor

The final control scheme presented in this work is for the TMA. Here, there are no particular considerations, because the system is easier than the EHA one. The starting point of the tuning is the EA control, because the systems are similar to some extent.

5.3.1 Requirements

The requirements for this control scheme are listed in Table 5.6. As can be seen, there are no particular constraints. The rise times for the controllers are chosen by directly inspect the open-loop simulation plots.

Requirement	Value	Units
Phase margin	60°	
Gain margin	6	dB
Current rise time	0.76	s
Desired frequency of current loop	8.267	rad/s
Velocity rise time	1.5	s
Desired frequency of velocity loop	4.188	rad/s
Position rise time	4	s
Desired frequency of position loop	1.57	rad/s
Maximum supply voltage	±415	V

Table 5.6: TMA — Control requirements

5.3.2 Design and simulation

The scheme of this control is almost the same is similar to the one of the EA; a rack position control outer-loop, an inner motor velocity loop, and an innermost motor current control loop.
In contrast to the EA the motor current control loop is controlled by a PI controller. The parameters are found by respecting the frequency and time requirements.
In Figure 5.13 and Figure 5.14 the results of the simulation are shown.

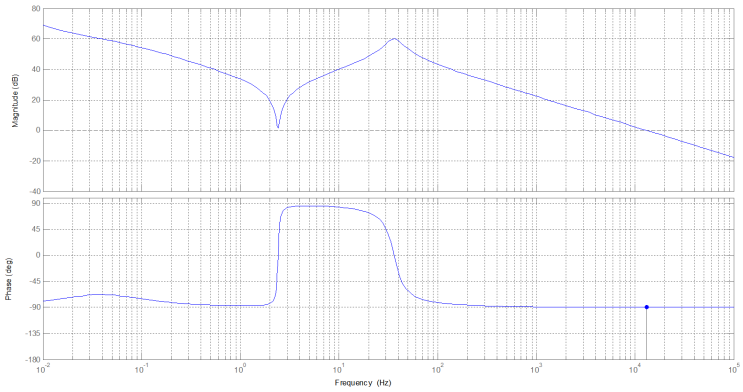

Figure 5.13: TMA - Frequency response current control loop. $PM = 90.1$, $GM = \infty$

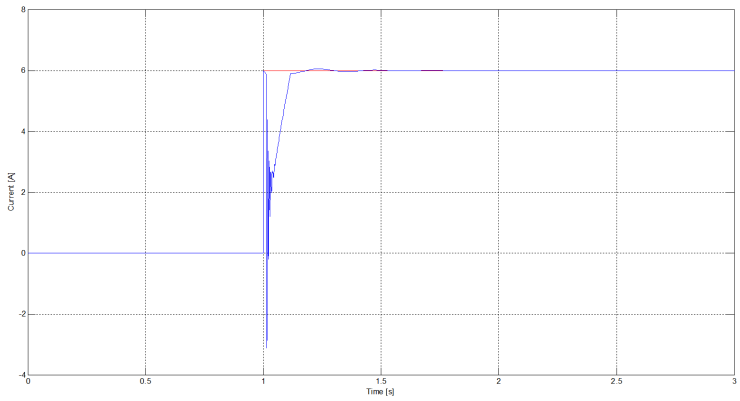

Figure 5.14: TMA — Step response of the current control. The red curve is the set point, instead the blue profile is the measure variable

In these pictures one may notice as the stability margins are not exceeded ($PM = 90.1$, $GM = \infty$) and how the set-point is finally reached.
Outside the previous control, another PI is used to control the motor velocity. Even in this situation, the parameters fulfil the requirements for frequency and time domain. These can be seen in Figure 5.15 and Figure 5.16.

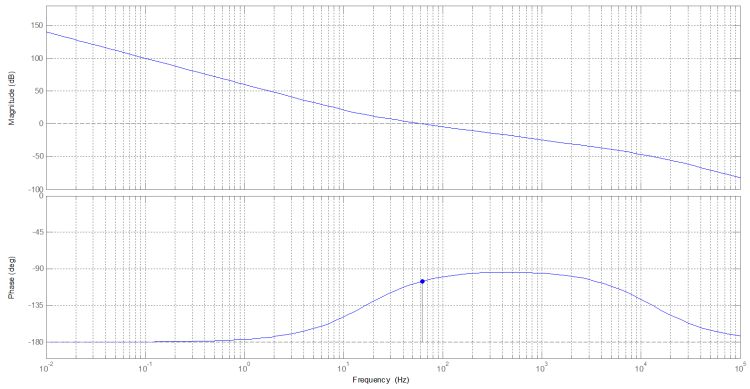

Figure 5.15: TMA — Frequency response velocity control loop. $PM = 74.7$, $GM = \infty$

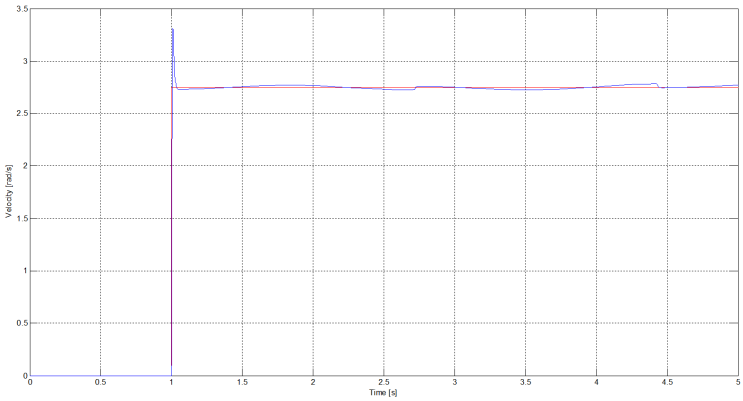

Figure 5.16: TMA — Step response of the velocity control. The red curve is the set point, instead the blue profile is the measure variable

Also for the velocity control, all the stability margins are not exceeded ($PM = 74.7$, $GM = \infty$) and the set-point is reached apart from a little remaining steady-state error, as can be seen in the previous pictures.
The final control is a PI tuned in the same way as the other actuators. In Figure 5.17 and Figure 5.18 the simulation results.

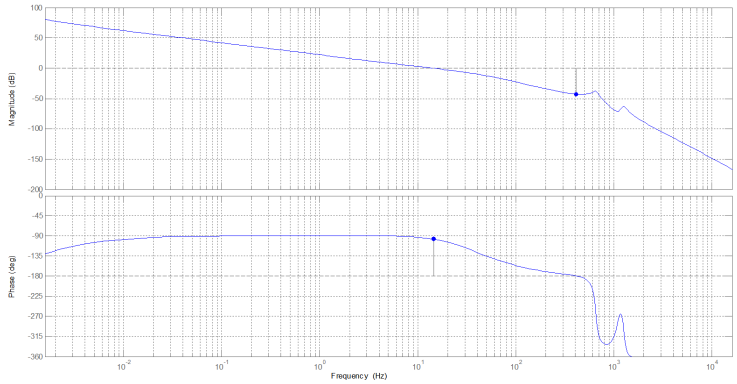

Figure 5.17: TMA — Frequency response position control loop. $PM = 83.5$, $GM = 43dB$

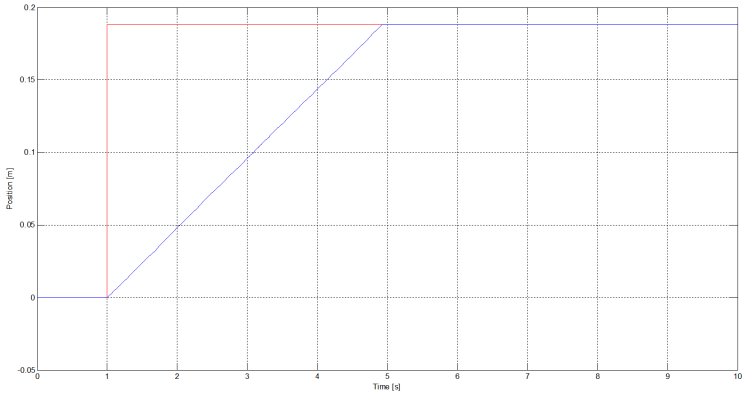

Figure 5.18: TMA — Step response of the position control. The red curve is the set point, instead the blue profile is the measure variable

In these last figures it can be noticed that all the stability margins ($PM = 83.5$, $GM = 43dB$) are fulfilled, together with the other requirements as no overshoots or zero steady-state error.

All the parameters used for these controls are summarised in Table 5.7.

Parameters	**Symbol**	**Value**
Current loop proportional gain	K_{pc}	83
Current loop integral time constant	τ_{ic}	0.009 s
Velocity loop proportional gain	K_{pv}	10
Velocity loop integral time constant	τ_{iv}	0.009 s
Position loop proportional gain	K_{pp}	100
Position loop integral time constant	τ_{ip}	90.73 s

Table 5.7: TMA — Control parameters

Chapter 6

Simulation Results

In the previous chapters the descriptions of each actuator are shown. For each solution were presented the models of the real actuator and the related mechanical linkage. After this, a simplified control schemes were designed.
This chapter will present the final comparison between the three actuators. In order to compare these systems some considerations have to be made.
Firstly, a single movement of the switch rails is considered, because it is the most common movement, performed by a switch. Moreover, a different choice will not change the conclusions, because even if the values change the differences with the other actuators remain the same. Hence, for simplicity, all the simulations were done asking for a single movement. However, a figure showing a double movement (i.e., when three routes are present and the switch moves to times to open the more distant route) simulation is shown in each section for a complete work.

Secondly, three different real scenarios are taken into account to have data for a more accurate analysis on the impact of these switches in a real railway network.

6.1 Performances comparison

The final comparison between the actuators is made looking at the different characteristics or data, as explained in Chapter 2:

- Velocity of the actuator
- Electric power consumption
- Physical dimensions

These three characteristics are able to show the most significant differences between the solutions.

6.1.1 Velocity comparison

The first comparison it has to be on the velocity of actuation. In fact, this is one of the main benefits of a REPOINT switch. In Figure 6.1 and Figure 6.2 the rail deflections, the lateral and the vertical one, of each actuator are shown.

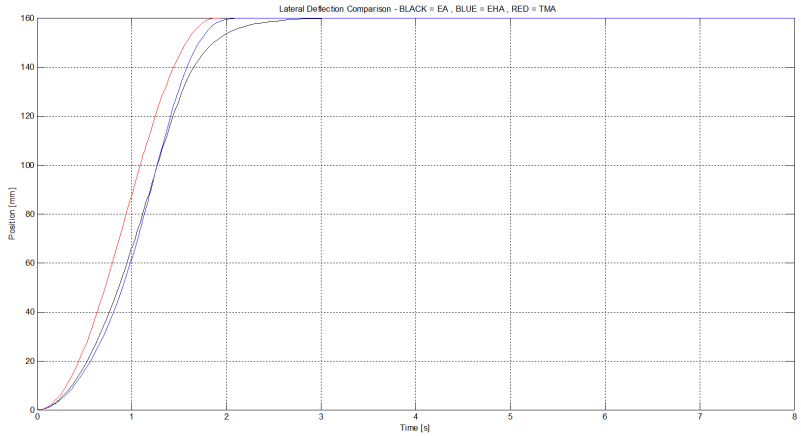

Figure 6.1: Comparison of the lateral deflection of the barer of each actuator model. (Black curve) EA, (Blue curve) EHA, (Red curve) TMA. The curves represent only a single movement of the switch rail

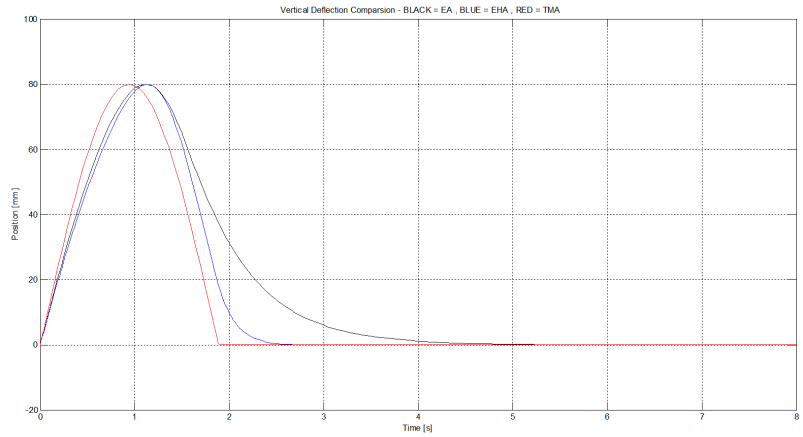

Figure 6.2: Comparison of the vertical deflection of the barer of each actuator model. (Black curve) EA, (Blue curve) EHA, (Red curve) TMA. The curves represent only a single movement of the switch rail

In these pictures EA is the black one, EHA is blue, and the red profile represents the TMA. As can be seen from these results, the differences in terms of velocity of actuation between the three actuators are not large. However, the torque motor one is the fast-

est. The electro-mechanical is the slowest one, but it is also notable that each actuator reaches the target of the REPOINT project: doing the movement of the switch rails in around two seconds.

In Figure 6.3 and Figure 6.4 the characteristics resulting from a double movement simulation are shown.

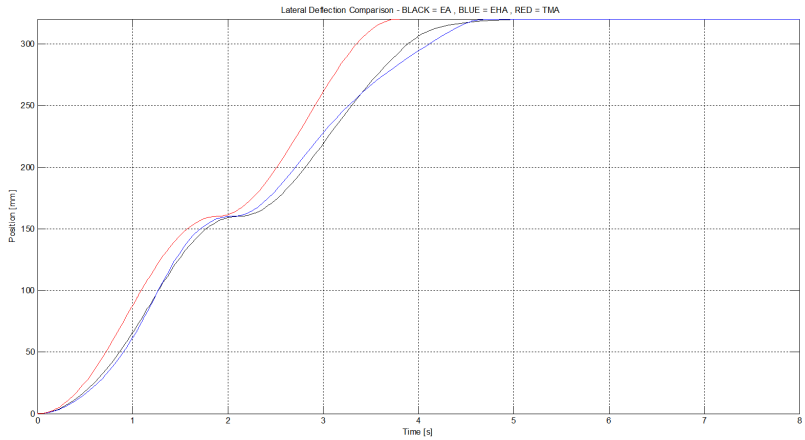

Figure 6.3: Comparison of the lateral deflection of the barer of each actuator model. (Black curve) EA, (Blue curve) EHA, (Red curve) TMA. The curves represent a double movement of the switch rail (i.e., when three routes are present and the switch moves two times to open the most distant route)

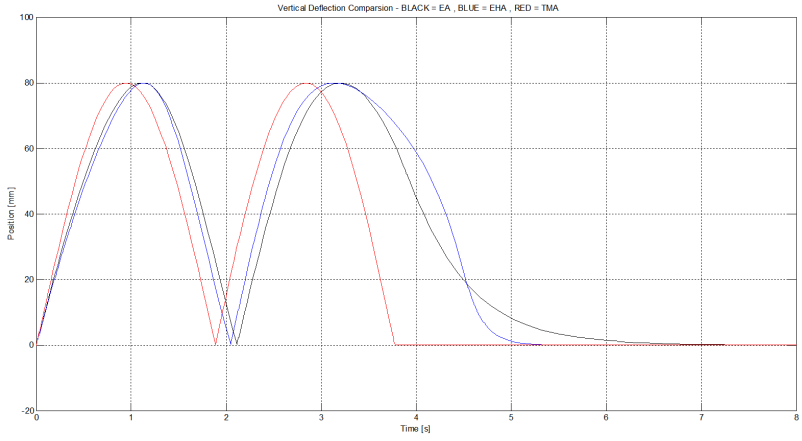

Figure 6.4: Comparison of the vertical deflection of the barer of each actuator model. (Black curve) EA, (Blue curve) EHA, (Red curve) TMA. The curves represent a double movement of the switch rail (i.e., when three routes are present and the switch moves two times to open the most distant route)

The results are different, but the differences among the actuator curves remain the same. TMA is still the fastest and the EA the slowest. The different profile is caused by the fact that in the second position there is a stronger rail deflection, which means greater reaction forces, as explained in Equations 4.10.

6.1.2 Electric power comparison

Another important factor in the comparison between the actuators is the electric power demand. Performing the movement of the rails with a small value of power is preferable a higher one.
In Figure 6.5 the profile of the electric power for the actuators is showed.

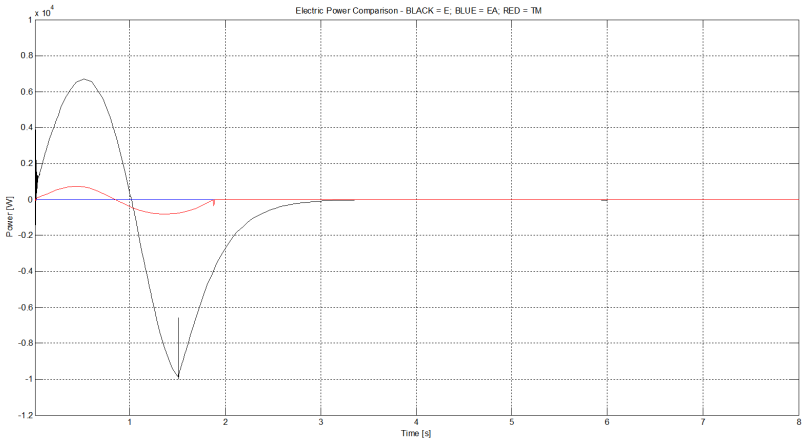

Figure 6.5: Comparison of the power demand for each actuator. (Black curve) EA, (Blue curve) EHA, (Red curve) TMA. The curves represent only a single movement of the switch rail

As in the previous section, a double movement simulation is made showing that there are not more differences than the single movement case. Figure 6.6 represents the three characteristics.

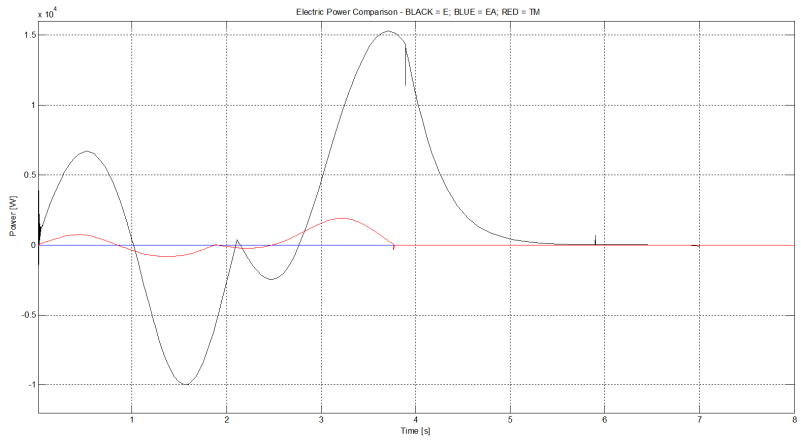

Figure 6.6: Comparison of the power demand for each actuator. (Black curve) EA, (Blue curve) EHA, (Red curve) TMA. The curves represent a double movement of the switch rail (i.e., when three routes are present and the switch moves two times to open the most distant route)

6.1.3 Physical dimensions comparison

Lastly, in order to have a reasonable comparison among the different actuation types, is important to have an idea around the physical dimensions. A larger actuator, indeed, could fit better or not depending on the space available in that particular location.
In Table 6.1 are reported the final results.

Parameter	**length x width x height**	**Units**
EA	408 x 141 x 147	mm
EHA	1664 x 220 x 221.4	mm
TMA	795 x 795 x 150	mm

Table 6.1: Comparison of the physical dimensions among the actuators

6.2 Real scenarios

In order to see a real impact of these actuators on a real railway network, three real scenarios are taken into account. They refer to three different cases, which outlines typical scenarios of a railway network. In this work two stations are considered, London Waterloo and Derby, and one junction, Weaver.
London Waterloo is chosen as an example of a very big and busy station in UK. Derby station may be considered as a busy intermediate junction between north and south of the United Kingdom. Weaver junction is an important and busy junction located a few kilometres far from Liverpool and away from all stations.

The aim of choosing these scenarios is to show the performances of the REPOINT switches in terms of power demand and dimensions. In a practical way, is found how many times in average there is a switch per hour. In order to do that, an approximate number of switches placed in the different cases are estimated. After this, an average of the number of trains passing through these junctions is found. This computation is made looking at departures and arrivals of the considered stations. These data are taken directly from the NATIONAL RAIL website [25], and they refer to peak times, so that a worst case may be analysed. The peak times is selected by comparing the results taken in different hours of the afternoon during the week. Another consideration is made concerning the trains frequency: by using this method to find the number of trains, all the freights are not taken into account. For this reason, a reasonable coefficient is considered. It is assumed that less than half of all trains passing through Derby station and Weaver junction are freights. Waterloo station is not affected by this problem, because is a terminal station, used only for passenger trains. Lastly, it is assumed that half of the switches are moved for each train.
In the following tables all the results of these evaluations are listed.

London Waterloo	
Peak time	18:00 - 19:00
# of switches	55
# of platforms	24
TOT transit trains	97
Switches per hour	2667.5

Table 6.2: London Waterloo Station — Results

Derby	
Peak time	18:00 - 19:00
# of switches	42
# of platforms	6
Passenger trains	32
Freight coefficient	0.4
TOT transit trains	44.8
Switches per hour	940.8

Table 6.3: Derby Station — Results

Weaver	
Peak time	17:30 - 18:30
# of switches	5
Passenger trains	13
Freight coefficient	0.4
TOT transit trains	18.2
Switches per hour	45.5

Table 6.4: Weaver Junction — Results

From Figure 6.5 it is possible to find the value of the power peak for the three devices. In Table 6.5 are reported these values.

Actuator	**Power Peak**	**Units**
Electro-mechanical	9.98	kW
Electro-hydraulic	0.0223	W
Torque motor	805.57	W

Table 6.5: Power peak for each actuator. The results are taken directly from Figure 6.5

The maximum installed power is an important data, which may be used to define the impact of this switch on a real network. In Table 6.6 the results for EA and TMA are listed. The values are evaluated by simply multiplying the peak of power of Table 6.8 by the number of switches in Tables 6.2, 6.3, 6.4.

Actuator	**London Waterloo**	**Derby**	**Weaver**
Electro-mechanical	548.9 kW	419.16 kW	49.9 kW
Torque motor	44.306 kW	33.833 kW	4.027 kW

Table 6.6: Max. installed power for each actuator in each scenario

A different computation may be made for the electro-hydraulic actuator. This actuator, as explained in Chapter 3, has to be provided by a power pack. These devices may be able to provide so large power that one or many different actuators are supplied. Obviously, a larger power pack demands more electric power than a little one. Moreover, the power demand of the hydraulic actuator is negligible compared to the power pack one. The power packs selected in this work are able to provide flow and pressure for one, twenty-nine (PEC 202) or sixty-four (PEC 302) turnouts. With the last two it is possible to cover all the switches with one or two of this devices.
The results according to these considerations are reported in Table 6.7.

Power Pack	London Waterloo	Derby	Weaver
CO1	165 kW	126 kW	15 kW
PEC 202	180 kW	180 kW	90 kW
PEC 302	315 kW	315 kW	315 kW

Table 6.7: Max. installed power for EHA, considering different power packs, in each scenario

Obviously, the values in these last tables represent the worst case, where all the switches of the junction or station are moving at the same time. This generally does not happens, in particular for big stations. However, it is always better to design a network using worst cases.

Another comparison can be done concerning power. In fact, an average number of switch movements per hour is evaluated. By multiplying this number by the power peak of each actuator in the scenarios, an energy value is obtained. It is the average power demand of the active switches in an hour. In Table 6.8 the results for the EA and the TMA are reported.

Actuator	London Waterloo	Derby	Weaver
Electro-mechanical	26.621 MW/h	9.389 MW/h	454.09 kW/h
Torque motor	2.148 MW/h	757.88 kW/h	36.65 kW/h

Table 6.8: Power demand for each type of actuator in each scenario per hour

As said before, the EHA is different, because three solutions are taken into account regarding its power pack. The results for the different power packs are listed in Table 6.9.

Power Pack	London Waterloo	Derby	Weaver
CO1	8.002 MW/h	2.822 MW/h	136.5 kW/h
PEC 202	8.278 MW/h	2.919 MW/h	141.2 kW/h
PEC 302	13.129 MW/h	4.63 MW/h	223.94 kW/h

Table 6.9: Power demand for EHA power pack in each scenario per hour

The possibility to use only few large power packs, instead of many little ones, may be useful, in particular when a great number of turnouts are utilised in a limited space. If these large power packs are used the dimensional matters have to be dealt with again. These devices are very large compared to a typical actuator.

6.3 Final considerations

In conclusion it can be asserted that each of these actuators presents advantages and disadvantages considering different scenarios.
For the velocity of actuation no great differences emerged, because all these actuators are able to achieve the rails movement in around two seconds, as shown in Figure 6.1 and Figure 6.2. A more accurate analysis reveals that torque motor actuator is the fastest compared to the electro-mechanical one, which is the slower. At the end, however, to complete this movement in two seconds or in two seconds and hundredth doesn't matter and is not relevant for the railway network capacity. This result is important if it is related to traditional points. The increasing of a REPOINT switch is consistent in this direction.
Concerning the electric power demand and the dimensions, more considerations can be made. In addition to the analysis of each actuator, the case studies have helped to do a more accurate comparison. In fact, scenarios influence the results deeply. The number of turnouts acting per hour in a particular station or junction may suggest utilising one actuator in spite of another one. In fact, as can be seen in Table 6.8 big stations mean great values in terms of power.
From a power point of view, the TMA is always the best solution, because it guarantees the movement demanding less power, contrary to the EA, which is always the worst choice, as can be seen in Table 6.8 and Table 6.9. The EHA, with its bigger power pack, is not a good solution in little junctions, or where there are not many switches. In these cases, in fact, big power packs are oversized as can be seen in Table 6.6 and Table 6.7 and most of the energy will be wasted.
However, power demand is not the only important consideration that may be done. Physical dimensions of these actuators have a notable role. The TMA even if has the greatest efficiency concerning power, is also bulky. Having a torque motor close to the turnout may be a problem, in particular if the point is located in a place where the available space is limited. For instance, in big stations, where a large number of switches is taken, one of the aims is to occupy as small area as possible. In this situation, a TMA is not the desirable solution. From this point of view, the EA and the EHA are better than the TMA. Indeed, the dimensions of these actuators are considerably smaller than the other actuator, as can be seen in Table 6.1. For the EHA the presence of the power pack has to be considered, because is not negligible, as Table 3.13 shows. For this reason the EA remains the best solution for those scenarios where large spaces are not available. London Waterloo station and Derby station are two of these situations. The number of switches is large with also a big number of routes, which makes preferable a more compact solution. Another advantage of the EA is its ease of use and assembly.
Concerning diagnostic and fault detection, not many considerations may be done, be-

cause it is difficult to have reasonable data without building a real plant. In fact, it is common use to do a big part of these analyses directly upon the real components. However, it may be reasonably affirmed that these aspects will be not particularly different from those of the REPOINT laboratory demonstrator. This is due to the fact that the components are almost the same, or the solutions do not present parts that influence these aspects.

As discussed in the introduction of this chapter, from a safety standpoint, there is no considerable differences among the different actuators and linkage solutions, because of the intrinsic safety of the REPOINT switch.

Conclusion

A comparative assessment of three different actuator and drive assembly for a novel track switch has being discussed in the present work. The purpose of this study was to identify and investigate a number of solutions for the REPOINT switch and provide an overview of the impact of these actuation systems in different scenarios.

The selected actuators where an electro-mechanical BLDC actuator (EA), an electro-hydraulic actuator (EHA) and a electro-mechanical torque motor actuator (TMA). Firstly, a model for each solution was derived from a first analysis of the physical behaviours of the actuator components. Then, another model is built for each mechanical linkage. Afterwards, all these models were implemented on MATLAB SIMULINK®using real parameters from manufacturers' datasheets. The cams and hopper assembly, which is the most innovative mechanical part of a REPOINT switch was discussed separately because of the fact it is a common part in all the different actuator systems. Once a model is provided, a simple control design is tuned by looking to the REPOINT performances. Data, from the model simulation or from the manufacturers' datasheets, were collected for the final comparison. Each actuator was compared to the others in terms of velocity of actuation, electric power demand and geometrical dimensions. Lastly, three illustrative scenarios were analysed, in order to determine the advantages and disadvantages of each solution in that particular situation. For this purpose, a busy terminal station like London Waterloo Station, a busy intermediate station like Derby Station, and a busy junction away from all stations like Weaver Junction, which will cover most of the typical scenarios, were discussed in this work. The final results show that the EA remains the best solution where the geometrical dimensions are the limiting factor; conversely, the TMA is better from a power point of view. The EHA, on the other hand, offers a good compromise between dimensions and power, especially where a great numbers of turnouts are present. It was also explained that all the other performances required for a REPOINT switch were not influenced by the usage of one actuator instead of another one.

Future work may investigate in a more detailed way these particular solutions. In fact, better-performing components may be selected in order to achieve all the tasks of a REPOINT switch in the best way. Moreover, a few different laboratory demonstrators

should be realised by implementing different actuators and drive solutions. Thus, a more accurate analysis and comparison may be done. At least, testing the real performance of a REPOINT switch in an existing railway network will provide more detailed information about the real impact of this novel turnout on the railway capacity, and also validate the EA model. The laboratory demonstrator is made without the presence of the switch rails. For this reason is not possible to completely validate the models.

Bibliography

[1] HS2. *High-Speed 2 rail network*. URL: http://www.hs2.org.uk/ (visited on 2014) (cit. on p. 1).

[2] S. Bemment, R. Dixon, R. Goodall and S. Brown. 'Redundantly engineered track switching for enhanced railway nodal capacity'. In: vol. 1. PART 1. 2013, pp. 25–30 (cit. on pp. 1, 5).

[3] E. Kassa. 'Simulation of dynamic interaction between train and tunrout'. thesis. Göteborg, Sweeden: Department of Applied Mechanics, Chalmers University of Technology, 2004 (cit. on p. 4).

[4] O. Publications. *Long turnouts*. URL: http://www.ostpubs.com/wp-content/uploads/2012/07/Turnouts_001.jpg (visited on 2014) (cit. on p. 5).

[5] S. Bemment, R. Dixon and R. Goodall. 'An evaluation of redundancy concepts for fault tolerant railway track switching'. In: vol. 8. PART 1. 2012, pp. 763–769 (cit. on pp. 5–6, 8).

[6] N. Wright et al. *The Performance and Control Requirements of a REPOINT Track Switch*. Loughborough University, United Kingdom: Control System Research Group, School of Electronic, Electrical & System Engineering, 2014. in press (cit. on pp. 7–8, 10, 29, 50).

[7] V. W. Eveleigh. *Introduction to control systems design*. McGraw-Hill electrical and electronic engineering series. McGraw-Hill, 1972 (cit. on pp. 9, 50).

[8] AKM. Servomotor. KOLLMORGEN. URL: http://www.kollmorgen.com/en-us/products/motors/servo/akm-series/_literature/kollmorgen_akm_servomotor_selection_guide_en-us_revb/ (visited on 2014) (cit. on p. 18).

[9] Value TRUE. Planetary Gearheads. THOMSON MICRON. URL: http://www.kollmorgen.com/en-us/products/gearheads/planetary/_literature/true_planetary_gearheads_catalog_en-us/ (visited on 2014) (cit. on p. 18).

[10] N. Wright. 'The REPOINT Simulation Model'. Loughborough University, United Kingdom, Feb. 2014. in press (cit. on pp. 18, 22, 43, 47–48).

[11] CR. Steel Spur Rack. HPC. URL: http://www.hpcgears.com/pdf_c33/22.3.pdf (visited on 2014) (cit. on pp. 22, 33, 39).

[12] ST4. Steel Pinion Shaft. HPC. URL: http://www.hpcgears.com/pdf_c33/20.6-20.9.pdf (visited on 2014) (cit. on pp. 22, 33, 39).

[13] YG4. Spur Gear. HPC. URL: http://www.hpcgears.com/pdf_c33/23.68-23.73.pdf (visited on 2014) (cit. on pp. 22, 39).

[14] MOOG. *Electrohydraulic Valves ... A Technical Look*. URL: http://www.moog.com/literature/ICD/Valves-Introduction.pdf (visited on 2014) (cit. on p. 24).

[15] C. de Silva. *Sensors and Actuators: Control System Instrumentation*. Taylor & Francis, CRC, 2007 (cit. on pp. 25, 31).

[16] A. Morse. *Electrohydraulic servomechanisms*. McGraw-Hill, 1963 (cit. on p. 26).

[17] J. Hydraulic. *Hydraulic Cylinder: Double acting, double rod cylinder*. URL: http://www.jwhydraulic.net/images/double-acting-double-rod-cylinder-b1.jpg (visited on 2014) (cit. on p. 28).

[18] 760. Servo-valves. MOOG. URL: http://www.moog.co.jp/literature/ICD/760seriesvalves.pdf (visited on 2014) (cit. on pp. 29–30).

[19] CGH1. Hydraulic cylinder mill type. BOSH REXROTH. URL: http://www.boschrexroth.com/ics/content/UpToDate/PDF/re17332_2013-07.pdf (visited on 2014) (cit. on pp. 29–30).

[20] CO. Compact power units. HYDAC. URL: http://www.hydac.com/fileadmin/pdb/pdf/PRO00000000000000000000005306010011.pdf (visited on 2014) (cit. on pp. 30–31).

[21] PEC. Power Unit. HAGGLUNDS. URL: http://www.hagglunds.com.tw/DownloadFile/Hagglunds/PEC.pdf (visited on 2014) (cit. on pp. 30–31).

[22] TMB. Torque Motor. ETEL. URL: http://www.etel.ch/fileadmin/PDF/Products/TorqueMotors/TMB/TMB0760/TMB0760-070.pdf (visited on 2014) (cit. on pp. 36–37).

[23] C. Caprani. *Selection and performance criteria for electro-hydraulic servo-drive*. URL: http://www.colincaprani.com/files/notes/SAIII/Macaulay's%20Method%201011.pdf (visited on 2014) (cit. on p. 44).

[24] *B.S. 248*. British standard light flat bottom rails for use in mines. British Standard. 1926 (cit. on pp. 46–47).

[25] T. I. S. LIMITED. *National Rail - Live departures/arrivals*. URL: http://www.nationalrail.co.uk/times_fares/ldb.aspx (visited on 2014) (cit. on p. 70).